TURUN
YLIOPISTO
UNIVERSITY
OF TURKU

Multi-spacecraft observations of large solar energetic particle events with an inner-heliospheric spacecraft fleet

Ghulam Ume Farwa

TURUN YLIOPISTON JULKAISUJA – ANNALES UNIVERSITATIS TURKUENSIS
SARJA – SER. AI OSA – TOM. 759 | ASTRONOMICA – CHEMICA – PHYSICA – MATHEMATICA | TURKU 2026

TURUN
YLIOPISTO
UNIVERSITY
OF TURKU

MULTI-SPACECRAFT OBSERVATIONS OF LARGE SOLAR ENERGETIC PARTICLE EVENTS WITH AN INNER-HELIOSPHERIC SPACECRAFT FLEET

Ghulam Ume Farwa

TURUN YLIOPISTON JULKAISUJA – ANNALES UNIVERSITATIS TURKUENSIS
SARJA – SER. AI OSA – TOM. 759 | ASTRONOMICA - CHEMICA - PHYSICA – MATHEMATICA | TURKU 2026

University of Turku

Faculty of Science
Department of Physics and Astronomy
Physics
Doctoral Programme in Exact Sciences

Supervised by

Prof. Dr. Rami Vainio
Department of Physics and Astronomy
University of Turku
Turku, Finland

Dr. Nina Dresing
Department of Physics and Astronomy
University of Turku
Turku, Finland

Reviewed by

Prof. Dr. Rositsa Miteva
Institute of Astronomy with National Astronomical Observatory
Bulgarian Academy of Sciences
Sofia, Bulgaria

Dr. Maher A. Dayeh
Southwest Research Institute
San Antonio, Texas, USA

Opponent

Prof. Dr. Norma Bock Crosby
Royal Belgian Institute for Space Aeronomy
Brussels, Belgium

ISBN 978-952-02-0627-7 (PRINT)
ISBN 978-952-02-0628-4 (PDF)
ISSN 0082-7002 (Print)
ISSN 2343-3175 (Online)
Painosalama, Turku, Finland 2026

To my dearest mother, SABIRA PARVEEN, who taught me to believe in myself, to rise after every fall, and to keep chasing my dreams no matter the distance

UNIVERSITY OF TURKU
Faculty of Science
Department of Physics and Astronomy
Physics
FARWA, GHULAM UME: Multi-spacecraft observations of large solar energetic particle events with an inner-heliospheric spacecraft fleet
Doctoral dissertation, 134 pp.
Doctoral Programme in Exact Sciences
January 2026

ABSTRACT

Solar energetic particle (SEP) events are major manifestations of solar activity and present significant radiation hazards to space-based technology and human exploration. Despite extensive study, key questions persist regarding the contributions of flare- and shock-related acceleration, and the temporal evolution of SEP intensity profiles in the heliosphere. This thesis employs novel multi-spacecraft observations from early solar cycle 25 to advance understanding of SEP origin, acceleration, and transport, providing key insights for future space weather forecasting. The work is based on SEP events observed between November 2020 and May 2023 by Solar Orbiter, Parker Solar Probe, STEREO A, BepiColombo, and near-Earth spacecraft (SOHO and Wind). A new multi-spacecraft SEP event catalog was developed during the SERPENTINE project providing event parameters for $\sim$1 MeV and $\sim$100 keV electrons and $\sim$25 MeV protons, as well as for associated solar flares and type II radio bursts. The catalog comprises 45 independent multi-spacecraft events corresponding to $\sim$150 single-spacecraft observations, and was further extended during the thesis to include 98 events through December 2023. Electron and proton peak intensities were correlated to probe the roles of flares and shocks in SEP acceleration. Significant intensity correlations are found across the sample. Events from poorly-connected locations form a single SEP population, consistent with acceleration by spatially extended CME-driven shocks. Conversely, well-connected locations show two populations: one with a clear correlation between electron and proton intensities, linked to shock acceleration, and another, enriched in electrons, indicating a mixture of flare and shock-related acceleration. A superposed epoch analysis of normalized SEP intensity–time profiles for electrons and protons shows similar trends, generally well described by power-law or exponential functions. The similarity of these profiles, along with observed onset delays, supports the value of relativistic electrons as early indicators for forecasting later-arriving protons.
KEYWORDS: space physics, solar energetic particles, solar flares, coronal mass ejections, particle acceleration

TURUN YLIOPISTO
Matemaattis-luonnontieteellinen tiedekunta
Fysiikan ja tähtitieteen laitos
Fysiikka
FARWA, GHULAM UME: Multi-spacecraft observations of large solar energetic particle events with an inner-heliospheric spacecraft fleet
Väitöskirja, 134 s.
Eksaktien tieteiden tohtoriohjelma
Tammikuu 2026

TIIVISTELMÄ

Auringon korkeaenergisten hiukkasten purkaukset ovat keskeisiä Auringon aktiivisuuden ilmentymiä ja muodostavat merkittäviä säteilyriskejä avaruudessa toimivalle teknologialle ja ihmiselle avaruudessa. Laajasta tutkimuksesta huolimatta avoimeksi on jäänyt keskeisiä kysymyksiä hiukkaspurkausten laajuudesta, roihuihin ja iskuaaltoihin liittyvien kiihdytysprosessien suhteellisista osuuksista sekä hiukkaspurkausten intensiteettiprofiilien ajallisesta kehityksestä heliosfäärissä. Työssä hyödynnetään aurinkosyklin 25 alkuvaiheen uusia moniluotainhavaintoja. Tavoitteena on ymmärtää paremmin korkeaenergisten hiukkasten alkuperä ja kiihdytyksen ja kuljetuksen mekanismit sekä tarjota uusia menetelmiä tulevaa avaruussään ennustamista varten. Työ perustuu Solar Orbiterin, Parker Solar Proben, STEREO A:n, BepiColombon sekä Maan lähiavaruuden luotainten (SOHO ja Wind) havaitsemiin hiukkaspurkauksiin marraskuulta 2020 toukokuulle 2023. SERPENTINE-projektin aikana luotiin uusi moniluotainhiukkaspurkauskatalogi, joka sisältää purkausparametreja 1 MeV:n ja 100 keV:n elektroneille, 25 MeV:n protoneille sekä niihin liittyville roihuille ja tyypin II radiopurkauksille. Katalogi sisältää 45 itsenäistä moniluotainhiukkaspurkausta ja noin 150 yksiluotainhavaintoa näistä. Katalogia laajennettiin vielä työn aikana 98 hiukkaspurkaukseen sisältäen tapahtumat joulukuuhun 2023 saakka. Elektronien ja protonien huippuintensiteettien korrelaatiota tarkasteltiin roihuja iskuaaltokiihdytyksen roolien selvittämiseksi. Merkittäviä intensiteettikorrelaatioita havaittiin koko aineistossa. Heikosti magneettisesti kytkeytyneistä sijainneista peräisin olevat purkaukset muodostavat yhden populaation, joka on sopusoinnussa laaja-alaisten koronan massapurkausten ajamien iskuaaltojen tuottaman kiihdytyksen kanssa. Hyvin kytkeytyneissä sijainneissa taas näkyy kaksi populaatiota: yksi, jossa on selkeä korrelaatio elektronien ja protonien intensiteettien välillä viitaten iskuaaltokiihdytykseen, sekä toinen, jossa elektronit ovat rikastuneet viitaten roihuja iskuaaltoperäisen kiihdytyksen sekoitukseen. Normitettujen intensiteettiprofiilien päällekkäisten epookkien analyysi elektroneille ja protoneille osoittaa samankaltaisia trendejä. Ne ovat hyvin kuvattavissa potenssilaeilla tai eksponenttifunktioilla. Profiilien samankaltaisuus yhdessä havaittujen alkuaikaviiveiden kanssa tukee relativististen elektronien käyttöä myöhemmin saapuvien protonien ennustamisen.

ASIASANAT: avaruusfysiikka, auringon korkeaenergiaiset hiukkaset, auringonpurkaukset, koronan massapurkaukset, hiukkaskiihdytys

Acknowledgements

Completing this PhD project has been a long and challenging journey, and I am filled with gratitude for all who have guided and supported me, including those whose names may not appear here. Thank you from the bottom of my heart.

I am especially grateful to my main supervisor, Rami, for giving me the opportunity to pursue a PhD in space physics, a field that has fascinated me since my early education. Rami's willingness to give me a chance, despite my background in experimental plasma and nano-technology and my return to research after years of teaching, laid the foundation for this work. Throughout my doctoral studies, he guided me through the fundamental concepts and analysis techniques of the field, helping me develop a strong scientific understanding and confidence as a researcher. I acknowledge the EDUFI grant and subsequent funding arranged for this project. His guidance and support in all aspects of this project has been instrumental in shaping both my research and my development as an independent researcher. I feel truly privileged to have learned from and worked alongside such an extraordinary mentor. Thank you Rami!

I warmly thank my co-supervisor, Nina, for her constant guidance and support, for always being available for discussions, patiently assisting with data analysis and writing, and providing constructive feedback that greatly enhanced the quality of my work and deepened my confidence in my research abilities. I will always regard the support and guidance of Rami and Nina as a strong foundation for my future endeavors.

I am deeply honored that Dr. Norma Bock Crosby has accepted the role of opponent and is traveling to Finland for my thesis defence. I would also like to sincerely thank the pre-examiners, Dr. Rositsa Miteva and Dr. Maher A. Dayeh, for their valuable time, careful evaluation of this thesis, and insightful comments.

I would also like to sincerely thank all my co-authors for their invaluable contributions to this work. Their expertise, insightful discussions, and collaborative efforts greatly enriched the research and strengthened the quality of the publications.

Finally, I am grateful to all members of the Space Research Laboratory at the University of Turku for providing an inspiring and supportive working environment. I am especially grateful to Laura, Christian, and Seve for their invaluable support: Laura for her friendly guidance and for always being there to discuss ideas or help find solutions, and Christian and Seve for their assistance in developing my program-

ming and Python skills which greatly contributed to the progress of this work.

Above all, I thank my friends and family for their endless love and support. To my parents who have always been my source of strength and confidence, and to my beloved brother and sister, Gul and Banine, who believed in me even when I doubted myself—this achievement is as much yours as it is mine.

To my loving husband, Jarar, for his patience, unconditional love, and the sacrifices he made so I could pursue my career—your support and trust have been my anchor. To my wonderful children, Wali and Shandana, for their love, energy, and the countless moments they allowed me to be "away" yet never apart—you are the heart of all I do.

Turku, January 2026
Farwa

GHULAM UME FARWA
Ume Farwa (b. 1988 in Chakwal, Pakistan) received her Master of Philosophy in Physics from Quaid-i-Azam University, Pakistan, in 2011. She served as an Assistant Professor of Physics in the Higher Education Department of Punjab, Pakistan. She is currently a doctoral researcher at Space Research Laboratory, University of Turku, Finland. Her research focuses on data-driven characterization of solar energetic particles and its application in space weather forecasting.

Table of Contents

Abbreviations

3D	three-dimensional
3DP	Three-Dimensional Plasma and Energetic Particle Investigation
ACE	Advanced Composition Explorer
AI	Artificial Intelligence
au	astronomical unit
CC	Correlation Coefficient
CDAW	Coordinated Data Analysis Workshops
CGS	Centimeter-Gram-Second
CIR	Co-rotating Interaction Region
CME	Coronal Mass Ejection
CUSUM	Cumulative sum
DM	Deca-Metric
EPD	Energetic Particle Detector
EPHIN	Electron Proton Helium Instrument
EPI-Hi	Energetic Particle Instrument High energy telescope
EPI-Lo	Energetic Particle Instrument Low energy telescope
EPT	Electron Proton Telescope
ERNE-HED	Energetic and Relativistic Nuclei and Electron-Heavy Ion Detector
ESA	European Space Agency
EUV	Extreme UltraViolet
GLE	Ground-Level Enhancement
GOES	Geostationary Operational Environmental Satellite
HET	High-Energy Telescope
HXR	Hard X-ray
ICME	Interplanetary Coronal Mass Ejection
IP	Interplanetary
LASCO	Large Angle Spectroscopic Coronagraph Observatory
NASA	National Aeronautics and Space Administration
PCC	Pearson Correlation Coefficient
pfu	particle flux unit $(\mathrm{cm}^2\ \mathrm{sr}\ \mathrm{s})^{-1}$
PSP	Parker Solar Probe

SC	Spacecraft
SCC	Spearman Correlation Coefficient
SEA	Superposed Epoch Analysis
SEP	Solar Energetic Particle
SEPT	Solar Electron and Proton Telescope
SERPENTINE	Solar EneRgetic ParticlE aNalysis plaTform for the INner hEliosphere
SIR	Stream Interaction Region
SIXS-P	Solar Intensity X-Ray and Particle Spectrometer-Particle instrument
SOHO	Solar and Heliospheric Observatory
SOLER	Energetic Solar Eruptions: Data and Analysis Tools
STEREO	Solar TErrestrial RElations Observatory
STIX	Spectrometer Telescope for Imaging X-rays
SXR	Soft X-Ray
SWPC	Space Weather Prediction Center
UV	Ultra Violet

Symbols

k	kilo
M	Mega
G	Giga
eV	electron-volt
R	Heliocentric distance
L1	Lagrangian equilibrium point
Å	Angstrom
erg	Unit of energy in CGS system (1 erg $= 10^{-7}$ Joules)
$\Delta\Phi$	Longitudinal separation
Φ_{flare}	Longitude of flare
Φ_{SC}	Longitude of spacecraft magnetic foot point
m	meter
s	second
K	Kelvin
%	Percentage
W	Watt
Hz	Hertz

List of Original Publications

This dissertation is based on the following original publications, which are referred to in the text by their Roman numerals:

I N. Dresing, A. Yli-Laurila, S. Valkila, J. Gieseler, D. E. Morosan, G. U. Farwa, Y. Kartavykh, C. Palmroos, I. Jebaraj, S. Jensen, P. Kühl, B. Heber, F. Espinosa, R. Gómez-Herrero, E. Kilpua, V.-V. Linho, P. Oleynik, L. A. Hayes, A. Warmuth, F. Schuller, H. Collier, H. Xiao, E. Asvestari, D. Trotta, J. G. Mitchell, C. M. S. Cohen, A. W. Labrador, M. E. Hill and R. Vainio.
The solar cycle 25 multi-spacecraft solar energetic particle event catalog of the SERPENTINE project.
A&A, 2024; 687: A72.

II G. U. Farwa, N. Dresing, J. Gieseler, L. Vuorinen, I. G. Richardson, C. Palmroos, S. Valkila, B. Heber, S. Jensen, P. Kühl, L. Rodríguez-García and R. Vainio.
Electron and proton peak intensities as observed by a five-spacecraft fleet in solar cycle 25.
A&A, 2025; 693: A198.

G. U. Farwa, N. Dresing, J. Gieseler, L. Vuorinen, I. G. Richardson, C. Palmroos, S. Valkila, B. Heber, S. Jensen, P. Kühl, L. Rodríguez-García and R. Vainio.
Electron and proton peak intensities as observed by a five-spacecraft fleet in solar cycle 25 (Corrigendum).
A&A, 2025; 699: C2.

III G. U. Farwa, N. Dresing, L. Vuorinen, C. Palmroos, J. Gieseler and R. Vainio.
Superposed epoch analysis of solar energetic particle events observed in solar cycle 25.
Advances in Space Research, 2026; 77: 1304-1320.

1 Introduction

The Sun is an active star with its core temperatures near $1.5\,10^7$ K. The solar corona is the outer boundary of the atmosphere of the Sun, where we observe solar phenomena such as coronal holes, solar flares, and coronal mass ejections (CMEs). The solar mass mainly consists of about 73.5% hydrogen, 24.9% helium, 0.8% Oxygen, 0.3% Carbon, and 0.5% other remaining elements. Because the Sun is composed of hot plasma, it has a differential rotation. Near the equator, it completes one rotation every 25 Earth days, while near the poles, a full rotation takes roughly 36 days.

The extremely high coronal temperatures produce constant streaming out of charged particles, known as the solar wind (Bochsler, 2008). Beneath the surface of the Sun, the complex movements of plasma generate powerful magnetic fields that stretch outward with the solar wind, shaping both the solar atmosphere and the heliosphere. The solar activity varies throughout the 11-year solar cycle, reaching its peak during solar maximum, when numerous active regions host frequent and intense solar eruptions, including solar flares and CMEs. (e.g., Reames, 2021). During solar eruptions, energetic charged particles are emitted from the Sun with energies reaching up to GeV in the case of high solar activity (Vainio et al., 2009; Reames, 2015). These solar energetic particles (SEPs) propagate from the corona through interplanetary (IP) space along the magnetic field lines embedded in the solar wind. The SEP events having proton intensity >10 particle flux unit $(\mathrm{cm}^2\ \mathrm{sr}\ \mathrm{s})^{-1}$ (pfu) in >10 MeV proton energy range are considered as large SEP events and are important to be considered for space weather impact (Thakur et al., 2016; Papaioannou et al., 2016).

The most prominent and effective solar eruptions are solar flares, intense electromagnetic emissions from magnetic reconnection in active regions, and CMEs, which are large expulsions of magnetized plasma from the solar corona into the heliosphere; flares often accompany CMEs but can also occur independently (e.g., Reames, 1999). SEPs generated during such eruptions are typically accelerated either near the Sun in solar flares and coronal shocks or farther out in IP space by CME-driven shocks (Kahler et al., 2007; Kouloumvakos et al., 2015; Trottet et al., 2015; Papaioannou et al., 2016). These events are commonly categorized as “impulsive”, which are electron- and helium-rich, originate from flare-related magnetic reconnection, and display a narrow angular extent with good magnetic connectivity, or as “gradual”, which are generally linked to CME-driven shocks and are characterized by slower rises, longer durations, higher proton intensities, and broader longitudinal spread

(e.g., Kahler, 1992; Gosling, 1993; Tylka, 2001; Reames, 2013; Tylka et al., 1999; Tylka, 2001); however, recent research suggests that this distinction may be overly simplistic.

Many large SEP events are observed with such ion abundances and charge states that cannot be accounted for acceleration of the thermal solar wind alone suggesting the possibility of a pre-existing suprathermal particle population for injection into shock acceleration processes (e.g., Desai et al., 2003). Suprathermal particles are ions and electrons with energies higher than the thermal solar wind population energies which ranges between 1-2 keV and belong to multiple sources, including remnants of earlier SEP events, solar flares, and co-rotating interaction regions (CIRs) (Dayeh et al., 2009). Suprathermal particles play an important role as a seed population for the acceleration of SEPs. These particles have energies higher than the ambient solar wind but lower than typical SEP energies, making them easier to accelerate by processes such as magnetic reconnection during solar flare and CME-driven shock wave leading to more efficient acceleration. Hence, the composition and intensity of the suprathermal seed population strongly influence the characteristics and variations observed in SEP events (Desai et al., 2010; Desai and Giacalone, 2016; Bucik et al., 2022).

SEP intensity profiles, whose shapes vary by species and energy, provide valuable information about SEP origin, acceleration, and transport (Cane, 1985; Cane et al., 1988; Kecskemety et al., 2009; Dresing et al., 2014; Richardson et al., 2014); analyzing these variations helps disentangle flare and CME contributions and improves understanding of SEP propagation.

Magnetic connectivity between observer and source, typically described by the longitudinal separation between the magnetic field footpoints, is crucial in SEP analysis and strongly influences SEP characteristics, with some dependence on the observer's heliocentric distance (Lario et al., 2013; Richardson et al., 2014; Dresing et al., 2014; Rodríguez-García et al., 2023b). Well-connected events may involve both flare and shock acceleration, while poorly-connected events are more often dominated by shock-driven acceleration (Cliver and Ling, 2007; Farwa et al., 2025a, see footnote[1]).

Solar activity is closely related to the impact of space weather (Baker et al., 2013). Intense solar eruptions cause solar radiation storms having energetic protons with energies up to GeV that reach Earth's upper atmosphere, disrupting satellite navigation, damaging electronics aboard spacecraft (SC) and satellites (Iucci et al., 2005; Horne et al., 2013; Miteva et al., 2023), distorting high-frequency radio signals (Fiori et al., 2022). Solar storms also cause a radiation hazard to astronauts and

[1]This paper has a corrigendum (Farwa et al., 2025b) based on a correction to an error in data provided from the database. Hereafter, the original publication (Farwa et al., 2025a) together with the corrigendum (Farwa et al., 2025b) is cited as (Farwa et al., 2025a). The corrigendum (Farwa et al., 2025b) is cited separately only when specific details from it are required.

airline crews flying at high altitudes (Cucinotta et al., 2002; Getley et al., 2005). Therefore, an effective warning system is essential to predict SEP events and reduce such potential risks. SEP populations affecting the space weather are associated with both the flare and CME-driven shock acceleration and are important to study for forecasting tools (Klein and Dalla, 2017). Hence, a better understanding of the origin, acceleration, and transport mechanisms of SEPs is essential for improving the accuracy and reliability of space weather forecasting.

Despite significant research over the years, many scientific puzzles remain unresolved regarding the origin, acceleration, and transport of SEPs. This discrepancy is rooted in the complex interactions between injection, acceleration, and propagation processes that SEPs undergo in both the solar corona and IP space, making it difficult to develop a comprehensive understanding. Recent advancements in multi-spacecraft observations, enabled by spacecraft positioned at different heliocentric distances and helio-longitudes, offer a valuable opportunity to better characterize and disentangle the physical processes behind the origin and acceleration of SEPs. Still, there are many open questions in the field to be addressed. For example, Anastasiadis et al. (2019a) identify the most important questions as follow:

- How accurately can we identify the sources of energetic particles?

Since solar flares and fast CMEs often co-occur in large SEP events, and the impulsive phase of flare has a close temporal relationship with the early formation of CME-driven shocks in the low corona, it becomes difficult to distinguish between flare-related and shock-related contributions to particle acceleration (Kouloumvakos et al., 2015). Moreover, identifying shock signatures in the low corona, where high-energy particle acceleration is believed to begin, remains a challenge (Klimchuk, 2001), further complicating efforts to determine the dominant acceleration processes in the early phases of SEP events.

- How do coronal and IP transport processes alter the characteristics of the injected SEPs?

In general, the intensity profiles and energy spectra observed during an SEP event can reflect the characteristics of the particle source. However, as these energetic particles travel through the IP medium, they encounter various transport processes, along with magnetic turbulence, complex IP structures, and disturbed solar wind conditions, that modify their behavior. These transport effects make it difficult to directly trace the particles back to their source and accurately interpret their acceleration history (Masson, S. et al., 2012; Lario and Karelitz, 2014).

- How accurately can we characterize the magnetic connection between the SEP source and the observing spacecraft?

From the perspective of space weather forecasting Anastasiadis et al. (2019a) emphasize two fundamental questions that still need more satisfactory answers:

- Will a solar eruptive event result in an SEP event at Earth or elsewhere in the heliosphere?
- Which characteristics of the source solar eruptive event can be used to accurately predict SEP properties at specific locations?

A related key issue is whether CME parameters alone are sufficient for reliable SEP forecasting, or if flare-related information must also be considered to improve forecast accuracy (Klein and Dalla, 2017).

The research in this thesis is a contribution to improving the understanding of open science questions about SEPs. In particular, this thesis addresses the following major science questions:

- What is the relative potential contribution of the flare versus the CME-driven shock in producing large SEP events?
- Are the acceleration processes the same for electrons and protons?
- How does the potential acceleration source vary with the magnetic connection of the observer?
- How can an average SEP event be characterized and how does it differ for electrons and protons?

This thesis presents the statistical analysis of large SEP events observed in the early phase of solar cycle 25. Chapter 2 provides an overview of solar eruptions and explains their significance in the acceleration and injection of particles into IP space. Chapter 3 introduces the SEPs, in detail. In Chap. 4 the data and analysis methods used for the study are discussed. Chapter 5 summarizes the original publications included in this dissertation, and Chap. 6 concludes the results.

2 Solar Eruptions

2.1 Solar flares

Solar flares are dynamic outbursts from the Sun, first noticed independently by Carrington and Hodgson back in 1859 (Cliver, 2006). These magnetic events release energy over the electromagnetic spectrum, ranging from low-frequency radio waves up to high-energy gamma rays. They are often accompanied by other solar activity, like CMEs and SEPs (Kahler, 1992). Solar flares typically occur when magnetic reconnection takes place, most often within large, unstable active regions that are rapidly evolving and have complex magnetic structures (Schrijver, 2009). During reconnection, built-up magnetic energy is suddenly released and converted into kinetic and thermal energy (Priest and Forbes, 2002). A standard model of a solar flare formation (Shibata et al., 1995) is presented in Fig. 1.

At the magnetic reconnection point, the inward flow of comparatively cool plasma from the sides of magnetic loops and the ejection of hot plasma upward and downward are represented by blue and green solid arrows, respectively (Fig. 1). The black helices at the bottom represent the motion of electrons and ions accelerated during the initial phase of reconnection, moving along closed magnetic field lines toward the footpoint of the magnetic loop, where they trigger the emission of hard X-rays (HXR) and gamma rays. As these charged particles decelerate, they deposit energy into the plasma, causing heating and evaporation that injects plasma mass into closed loops (magenta arc) and produces soft X-ray (SXR) emission (Shibata et al., 1995).

A typical solar flare follows a three-phase evolution. The precursor phase is marked by small-scale brightening in ultraviolet (UV) and SXR wavelengths, indicating the onset of magnetic energy release and associated SXR emission. The impulsive phase releases most of the magnetic energy and is characterized by bursts of radio waves and HXR emissions, indicating strong acceleration of electrons and ions. HXR and microwave emissions originate from the same population of high-energy electrons through electron-ion bremsstrahlung and gyro-synchrotron radiation, respectively, while gamma-ray and white-light emissions are typically observed only in extreme flares during this phase. Solar flares are highly efficient at accelerating particles, with a significant fraction of the released magnetic energy converted into this process (Warmuth, 2015). SEPs are most likely energized at the flare site during the impulsive phase of magnetic reconnection involving open magnetic field lines, after

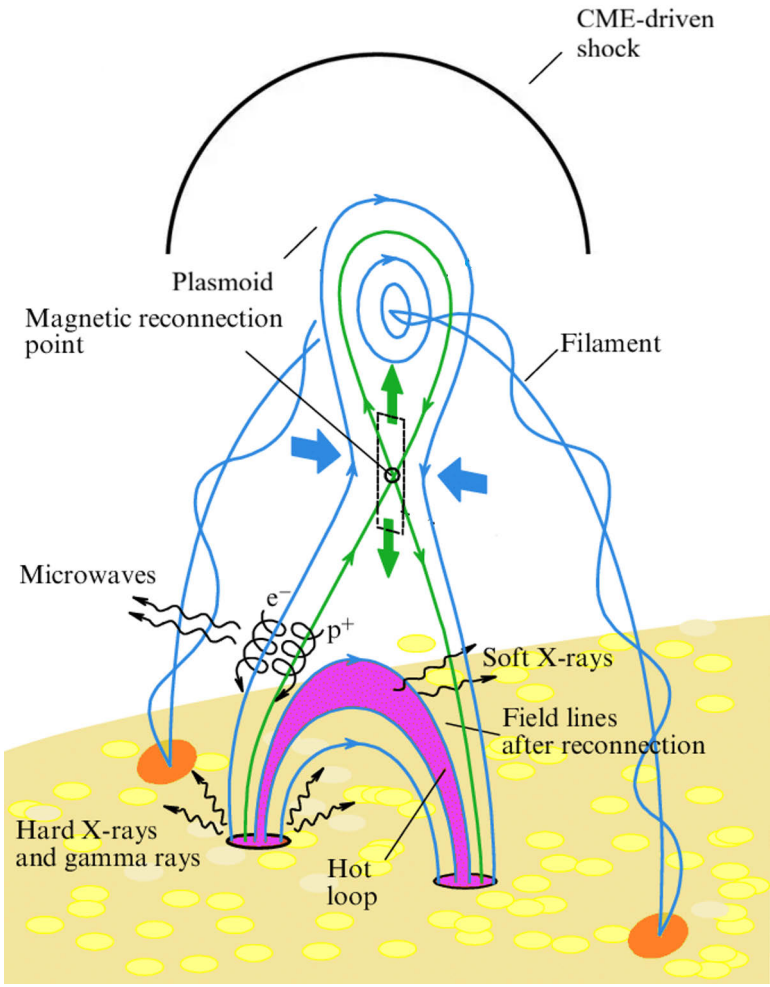

Figure 1. Standard model of a solar flare triggered by the magnetic reconnection (Shibata et al., 1995). Magnetic field lines of opposite polarity reconnect at a point represented by a black circle at the center. The blue and green solid arrows represent the plasma flow in and outward of the reconnection point, respectively. Black wavy arrows at the bottom represent the emission of HXR and gamma rays triggered by the acceleration of energetic electrons and protons along the closed magnetic field lines. The magenta arc represents the closed plasma loop where plasma heating takes place, resulting in SXR emission. The black curve represents the CME-driven shock wave. Image credit: Adapted from Lysenko et al. (2019).

.

which they propagate along these field lines through the solar corona and IP space, sometimes reaching Earth. Electron energies range from 10 keV to a few MeV, while protons can reach energies from several MeV up to multiple GeV (e.g., Kahler, 1992; Reames, 1999, 2002). The gradual phase is characterized by a slow decline in SXR and microwave emissions, during which bright loops and arcades become visible in SXR and extreme UV and may expand due to chromospheric evaporation. These phases can last from a few seconds to over an hour, depending on flare intensity (Bai and Sturrock, 1989).

The number of solar flares we observe changes with the timeline of a solar cycle. During solar maximum, several flares can erupt each day, while during solar minimum, they might occur less than once a week. Stronger flares are also much rarer than weaker ones (e.g., Kahler, 1992). Solar flares are generally divided into five classes; A, B, C, M, and X, based on the peak intensity of their SXR emissions, as measured by the Geostationary Operational Environmental Satellites (GOES) in the 1–8 Å wavelength range (Miteva, 2020). The scale is logarithmic: A-class flares are the weakest at 10^{-8} Wm^{-2}, and X-class flares are the strongest, exceeding 10^{-4} Wm^{-2} (Bai and Sturrock, 1989).

The most intense solar flare on record is believed to be the one associated with the 1859 Carrington Event. Based on the estimate of a ground-based magnetometer, it would have ranked around X45 on the SXR scale. In more recent times, the strongest flare measured with modern instruments occurred on November 4, 2003. It was so powerful that it saturated the GOES detectors, and its strength is estimated to be roughly X28 (Cliver and Dietrich, 2013).

2.2 Coronal mass ejections

A CME is a massive release of magnetized plasma from the solar corona, primarily made up of electrons and ions, and flown out into the heliosphere (Dayeh, 2015). These ejections generally involve mostly closed magnetic field lines and transport both plasma and magnetic flux into IP space (e.g., Kahler, 1992). The earliest optical detection of a CME occurred on December 14, 1971, using the coronagraph aboard the satellite named Orbiting Solar Observatory-7 (Tousey, 1973). These magnetic outbursts release roughly 10^{32} ergs of energy and eject an average plasma mass of around $1.6\,10^{12}$ kg into the IP medium. The size and shape of CMEs differ significantly from one event to another (Hernandez Camero et al., 2025). Their speeds range from about 100 $\mathrm{km\,s}^{-1}$ to over 3000 $\mathrm{km\,s}^{-1}$, with a typical speed near 500 $\mathrm{km\,s}^{-1}$. As they approach Earth, their radial extent can reach up to 0.25 au (Webb and Howard, 2012).

CMEs originate in the lower corona, triggered by the sudden reconfiguration of solar magnetic fields through magnetic reconnection. They commonly occur near sunspot groups and are frequently associated with other solar activities, including so-

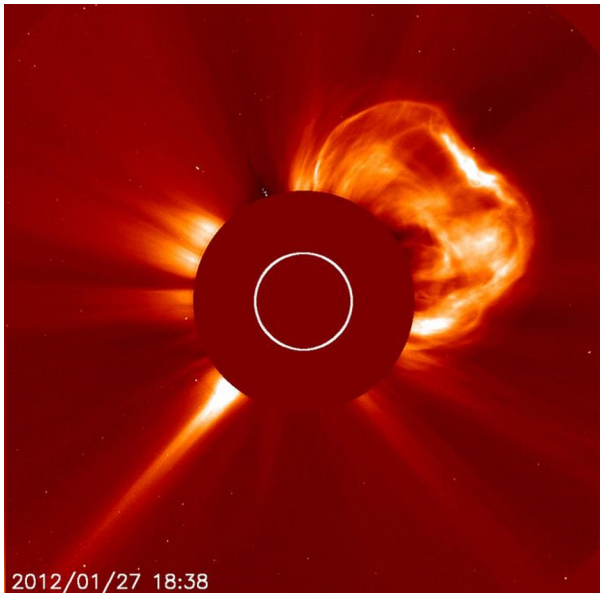

Figure 2. A typical CME in a Large Angle Spectroscopic Coronagraph Observatory (LASCO) coronagraph image. A solar disk covers the bright Sun and captures the mass ejection from the Sun. Image credit: ESA-NASA Solar and Heliospheric Observatory (SOHO) / LASCO.

lar flares and eruptive prominences (e.g., Kahler, 1992). However, flares and CMEs do not always erupt at the same time. The likelihood that a flare is accompanied by a CME increases with the flare's intensity; the intense flares are mostly associated temporally with a CME (e.g., Reames, 1999). The frequency of CMEs varies significantly throughout the solar cycle, with activity ranging from about two to three events per week during solar minimum to as many as five to six per day at solar maximum (e.g., Lugaz et al., 2017).

CMEs are observed using coronagraphs, which covers the bright solar disk to reveal faint structures around it. A typical CME observed by the LASCO coronagraph is represented in Fig. 2. CME detection relies on Thomson scattering of the photospheric photons by the electrons of the ejected plasma, an effect too faint to detect without occulting the bright solar disk. However, coronagraph cannot distinguish whether a CME originates from the front side (facing Earth) or backside (facing away from Earth) of the Sun (Hernandez Camero et al., 2025). These coronagraphs produce a view which is actually a two-dimensional projection of the three-dimensional structure of a CME onto the plane of the sky. As a result, measurements such as angular width, height, and speed of a CME and also its derived estimates like mass and energy, are the projected measurements and typically reflect only the lower bounds of their true values. Accurately determining the full three-dimensional (3D) characteristics of a CME remains a significant challenge (Vršnak et al., 2007). Al-

though combining LASCO chronographs with Solar TErrestrial RElations Observatory (STEREO) A, B coronagraphs made it possible to have a better 3D visualization of CME structure with reduced projection effects (Hutton and Morgan, 2017). The latest Metis chronographs of Solar Orbiter provide an additional view point out of the ecliptic plane to significantly improve the 3D reconstruction of CMEs, particularly for the shape, orientation, and expansion (Zimbardo et al., 2023).

A CME typically displays up to three distinct sub-structures: a bright leading edge, a dark cavity, and a bright core. The leading edge consists of compressed plasma pushed outward during the early stages of expansion, situated in front of the magnetic flux rope of CME. The cavity is thought to represent the prominence cavity, appearing as a magnetic flux rope viewed from the side. The bright core is associated with the erupting solar prominence. CMEs are categorized by their kinematics into two types: slow or gradual CMEs, which travel at speeds below 400 $\mathrm{km\,s^{-1}}$ and tend to accelerate over time, and fast or impulsive CMEs, which may exceed 2000 $\mathrm{km\,s^{-1}}$ and typically decelerate as they propagate (e.g., Kahler, 1992). Classification based on angular width includes halo, partial halo, and limb CMEs. A halo CME appears in coronagraph images as a bright, expanding ring that completely encircles the occulting disk. If the ring covers more than 120° but does not fully surround the disk, it is termed a partial halo CME. CMEs with an angular width under 120° are known as limb CMEs. The speed and angular width of a CME serve as indicators of its overall intensity, with halo CMEs generally being the fastest and involving the most massive ejections (e.g., Gopalswamy et al., 2010). Once a CME travels beyond approximately 50 solar radii into IP space, it is referred to as an interplanetary coronal mass ejection (ICME) (e.g., Gosling, 1990).

Studies have shown a strong correlation between the characteristics of gradual SEP intensity-time profiles and the parameters of the associated CMEs, particularly their speed and angular width, indicating that gradual SEP events are primarily accelerated by CME-driven shocks (Kahler, 1982; Papaioannou et al., 2016; Dresing et al., 2022). On their interaction with Earth's magnetosphere, CMEs can cause severe magnetic storms, playing an important role in space weather (e.g., Gosling, 1993; Webb and Howard, 2012; Dayeh, 2015).

2.3 Shocks

When a CME moves faster than the local magnetosonic speed within the solar wind, it generates a shock wave ahead of it (Vourlidas et al., 2013). This phenomenon generally occurs for CMEs with speeds greater than 400 $\mathrm{km\,s^{-1}}$ in the lower corona and over 500–600 $\mathrm{km\,s^{-1}}$ in the heliosphere. The resulting shock precedes the CME front and expands outward through the solar corona and into the heliosphere. The typical formation of a shock wave ahead of a CME is represented in Fig. 3. A fast CME (yellow arc) with a magnetic flux rope (pink helical structure) with

both its legs still attached to the active region at the Sun generates a shock wave (black curve) in front of it. The region between the CME and the shock front, filled with compressed turbulent plasma, is called the sheath. As it propagates outward, this CME-driven shock gradually weakens due to solar wind expansion and geometric deformation of the wave front. Such shocks can reach 1 astronomical unit (au) or beyond, where they are observed as IP shocks (Lario and Decker, 2002; Santa Fe Dueñas et al., 2022; Cane, 1996). It should be noted, however, that IP shocks are not exclusively CME-driven; they can also arise from stream or co-rotating interaction regions (SIRs/CIRs) formed where fast solar-wind streams overtake slower ones (e.g., Gosling and Pizzo, 1999; Richardson, 2018); however, in this section we focus only on CME-driven shocks associated with eruptive events.

Remote sensing observations, for instance, white-light coronagraphs onboard the SOlar and Heliospheric Observatory (SOHO)/LASCO, reveal these shocks as faint, sharp fronts preceding the CME structures. In the extreme ultraviolet (EUV) range, imaging captures these shocks as "EUV waves", basically the low-coronal counterpart of CME-driven shocks, representing where the expanding shock wave intersects the lowest layers of the corona. The presence of type II radio bursts, generated by electrons accelerated at the shock front, provides further evidence of shock development and motion (Benz and Thejappa, 1988). Additionally, spacecraft instruments making in-situ observations identify shocks through abrupt variations in plasma characteristics, including sharp increases in solar wind speed, particle density, temperature, and magnetic field intensity.

CME-driven shock waves, together with solar flares, are a primary mechanism for accelerating SEPs (e.g., Reames, 1999). Ion acceleration at CME-driven shocks is commonly attributed to diffusive shock acceleration, in which particles gain energy through repeated crossings of the shock front (Axford et al., 1977; Krymskii, 1977; Bell, 1978; Blandford and Ostriker, 1978). These shocks can accelerate particles to high energies, modify the solar wind environment, and, upon reaching Earth's magnetosphere, trigger geomagnetic storms (e.g., Cane et al., 1988; Reames, 1999). Fast and wide CMEs spanning large longitudinal regions are particularly effective at driving shocks that accelerate particles and distribute SEPs over broad longitude ranges and large, gradual SEP events with enhanced proton intensities are closely associated with such shocks (e.g., Reames, 1999; Dresing et al., 2012, 2014; Lario et al., 2016, 2017; Rodríguez-García et al., 2021). Strong correlations have been reported between SEP peak intensities and various shock parameters (Kouloumvakos et al., 2019; Dresing et al., 2022), and the magnetic connection between the observer and the shock strongly influences SEP intensity profiles (Cane et al., 1988; Cliver et al., 1995; Cane et al., 2010; Lario et al., 2013; Dresing et al., 2022).

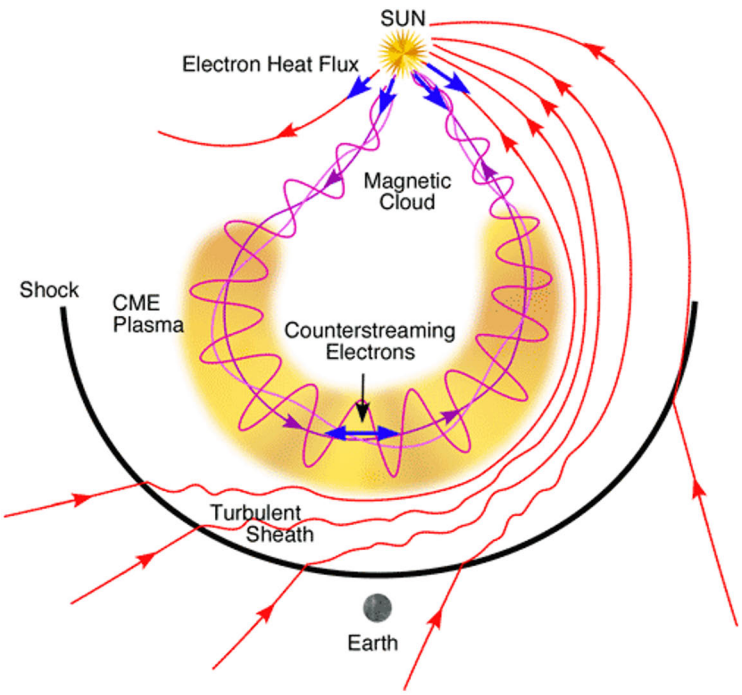

Figure 3. A typical schematic of a CME-driven shock wave. The yellow arc represents the CME loop embedded in the magnetic flux rope (pink helical structure) with both its legs connected to the source site at the Sun. The black curve represents the shock front driven ahead of the CME, while the region between the CME loop and the shock represents the sheath, a region of compressed and turbulent plasma. Image credit: Zurbuchen and Richardson (2006), reproduced with permission from SNCSC.

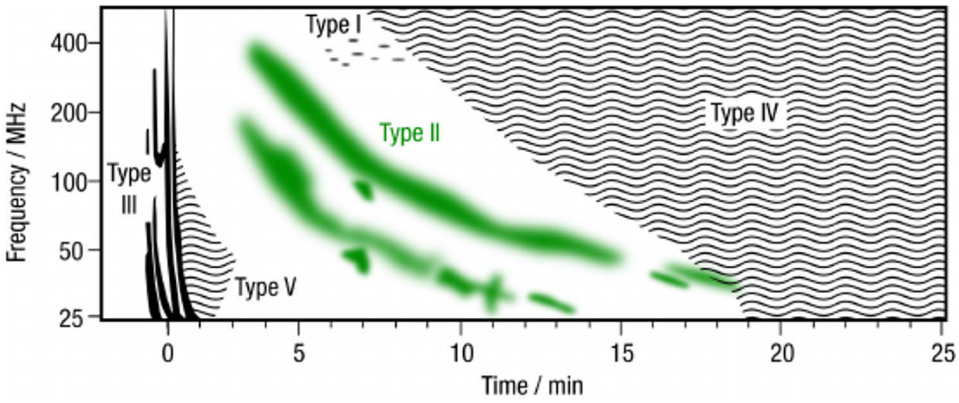

Figure 4. A typical classification of radio burst in a dynamic spectrum. Certain patterns of frequency-time profiles of radio emissions from the Sun characterize different types of radio bursts, represented as type I, II, III, IV, and type V radio bursts. Image credit: Ganse et al. (2012), reproduced with permission from SNCSC.

2.4 Radio bursts

Solar radio bursts are rapid, powerful emissions of radio waves originating mainly from the solar corona. They span a broad frequency spectrum, ranging from some kilohertz to several gigahertz. These phenomena are commonly associated with solar activity such as active regions, solar flares, and CMEs (White, 2024). Solar radio bursts are typically observed using ground-based radio telescopes fitted with specialized antennas capable of capturing radio waves emitted by the Sun. In addition to terrestrial observations, satellites in space can also detect these emissions. The first documented solar radio emission was reported in 1944, involving observations of 160 MHz radio waves signals originating from the chromosphere (Reber, 1944). However, the earliest known detection occurred in 1942, when British radar operators inadvertently observed solar radio signals during World War II (Kellermann et al., 2020).

The Sun generates radio emissions through four primary mechanisms, all of which involve the conversion of kinetic energy from energetic electrons into electromagnetic radiation. These mechanisms include thermal bremsstrahlung, gyromagnetic emission, plasma emission, and electron-cyclotron maser emission (Subramanian, 2010; Morosan et al., 2016). Each operates under different physical conditions and during various stages of solar eruptions, resulting in the diverse types of solar radio bursts observed (Sinclair and Heather, 2014; Morosan et al., 2019).

Solar radio bursts are mainly classified according to their morphology in dynamic spectra recorded by radio spectrographs, as well as their origin within the solar chromosphere and corona (Ganse et al., 2012; White, 2024). The typical morphology of radio burst is represented in Fig. 4. Type I bursts appear as short, intense spikes of

radio emission that usually occur in clusters known as noise storms. These storms are associated with active regions on the Sun and can persist from several hours to multiple weeks. They are detected at frequencies ranging from approximately 50 to 500 MHz (Gergely and Erickson, 1975). Type II bursts, in contrast, are characterized by a slow frequency change from high to low over several minutes. They often display two separate emission bands, corresponding to the fundamental and harmonic components of plasma emission originating from the same source. Plasma emission is a mechanism in which beams of non-thermal electrons excite plasma waves that are nonlinearly converted into escaping electromagnetic radiation at the plasma frequency or its harmonic (Li et al., 2021). Type II bursts are commonly associated with CMEs and are generated at the leading edge of CME where a shock accelerates electrons, triggering the plasma emission process (Kumari et al., 2023). Type II bursts are subdivided into different groups depending on the wavelength range observed for these bursts, called metric, decametric (DM), hectometric, and kilometric type II radio bursts. The metric and DM wavelength range corresponds to a frequency range of 30–300 MHz and 3–30 MHz, respectively (Aguilar-Rodriguez et al., 2005).

Type III bursts exhibit a very fast drift from higher to lower frequencies and are associated with electron beams up to tens of keV energy accelerated by magnetic reconnection during the early stages of solar flares (Sinclair and Heather, 2014). Type IV bursts consist of broad-band continuum emissions and are categorized into two types: moving and stationary. Moving type IV bursts are generally associated with gyro-synchrotron emission and/ or plasma emission, produced by fast electrons confined inside the magnetic fields of an erupting CME. In contrast, stationary type IV bursts are commonly observed emissions over a wide frequency range and are generally associated with solar flares or persistent type I activity (Morosan et al., 2019). Type V bursts are believed to result from harmonic plasma emission generated by the same fast electrons that produce type III bursts (Zheleznyakov and Zaitsev, 1968).

3 Solar Energetic Particles

SEPs are energetic charged particles, including electrons, protons and heavy ions, released by the Sun during solar eruptions. SEP events are characterized by significant increases in the flux level of protons, electrons, and heavier ions up to iron, with energies spanning from several tens of keV to multiple GeV, substantially exceeding the typical thermal energy of the solar wind (e.g., Vainio et al., 2009; Reames, 2021). During an SEP event, these particles are accelerated either at the Sun, within flaring regions and coronal shock waves, or farther out in IP space by shocks driven by fast CMEs. Once accelerated, SEPs escape the solar corona and travel through the IP space along open magnetic field lines, undergoing various transport processes (e.g., Anastasiadis et al., 2019b; Reames, 2021), eventually reaching Earth. The first indirect detection of SEPs occurred in 1942 when Scott Forbush observed energetic particles at ground level (Forbush, 1946).

3.1 Sources and classification of SEP events

Based on versatile characteristics, SEP events are classified into different types. SEP events are typically classified according to the energy levels of the detected particle species and their association with potential acceleration processes. An event is defined as a large SEP event when proton intensities exceed 10 particles $\mathrm{cm}^{-2}\,\mathrm{s}^{-1}\,\mathrm{sr}^{-1}$ (pfu) in the $>$10 MeV energy channel, as measured by GOES satellites (Mitra, 1974). Large SEP events can initiate solar radiation storms that directly affect space weather and pose threats to various technological systems (Iucci et al., 2005; Fiori et al., 2022). Additionally, they represent a significant radiation hazard to astronauts and aircrew operating at high altitudes (Cucinotta et al., 2002; Getley et al., 2005; Beck et al., 2005).

In particularly intense events, the energy of SEPs can reach several GeV, high enough to penetrate the magnetic field of Earth and reach into the atmosphere of Earth. Such high-energy SEP events, when detected by ground-based neutron monitors, are classified as ground-level enhancements (GLEs) (Forbush, 1946). GLEs represent the most energetic of SEP events, characterized by ions accelerated to relativistic energies. These particles cause an increase in solar cosmic ray intensity at the surface of Earth (Papaioannou et al., 2014).

The frequency of SEP events is closely associated with the phase of the solar cy-

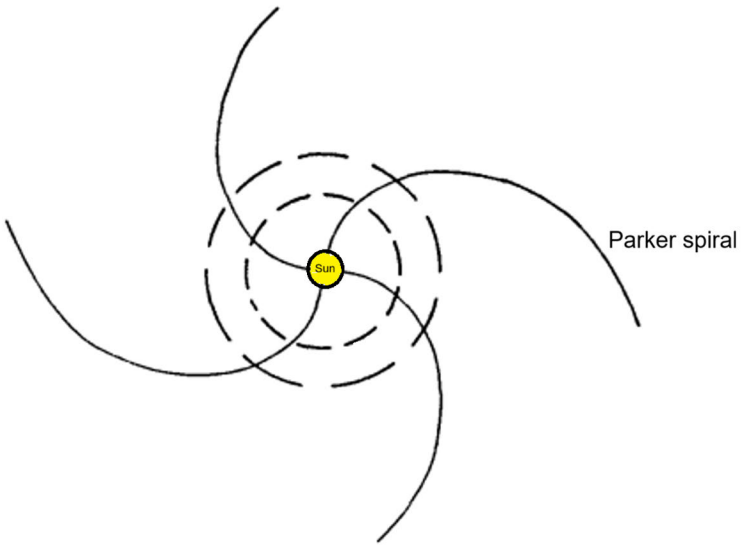

Figure 5. The drawing of the Parker spiral with the magnetic field lines twisted into a spiral due to radial outflow of solar wind and solar rotation. Image credit: Adapted from Parker (1958).

cle. During solar maxima, the larger number of active regions causes more frequent SEP events, while these events are less frequent during solar minima. Lower-energy SEP events occur relatively frequently, while large SEP events, those with higher energies (10–20 MeV), typically occur twenty to thirty times per year and can persist for several days. In contrast, GLEs are rare, occurring only a few per solar cycle and lasting from several minutes to a few hours (e.g., Anastasiadis et al., 2019b).

The observer's location relative to the source at the Sun plays a crucial role in classifying SEP events based on the magnetic connection from the Sun. This magnetic connection is described by the Parker model (Parker, 1958), which first proposed the solar wind and the spiral configuration of magnetic field lines. Due to high solar plasma conductivity, the magnetic field becomes embedded within the plasma, referred to as the field being "frozen-in" (Alfvén, 1942; Chang et al., 2022) and is carried outward by the solar wind. However, these lines, influenced by solar wind speed and solar rotation, do not extend radially but follow a spiral path known as the Parker spiral. Figure 5 adapted from Parker's original drawing (Parker, 1958), showing magnetic field lines spiraling outward from the Sun, carried by the solar wind.

The Parker spiral configuration is essential for understanding SEP transport, as SEPs mainly propagate along open magnetic field lines traced by these spirals (Parker, 1958; Chang et al., 2022). The magnetic connection from the observer to

the source is typically estimated by tracing a Parker spiral from the observer's location in IP space back to the footpoint on the solar surface (Gieseler et al., 2023). Longitudinal connectivity is quantified by the angular separation between the observer's magnetic footpoint and the source longitude. In general, an observer with a longitudinal separation $< 35^{\circ}$ is considered well-connected, while one with a separation beyond 35° is poorly-connected (Cliver and Ling, 2007; Lario et al., 2013; Núñez, 2018; Farwa et al., 2025a). Thus, SEP events are classified as well-connected or poorly-connected based on this magnetic separation (Cliver and Ling, 2007; Lario et al., 2013; Dresing et al., 2014, 2020; Farwa et al., 2025a), with further classification details provided in Sect. 4.2.3. The angular spread of SEP events mainly differs by origin: flares have a limited longitudinal extent (Kahler, 1977), while CME-driven shocks can reach wider longitudes. Well-connected events can display contributions from both flare and shock acceleration (e.g., Reames et al., 1996; Cliver and Ling, 2007; Farwa et al., 2025a), whereas poorly-connected events are more often dominated by shock-driven acceleration (Cane, 1985; Cane et al., 1988; Dresing et al., 2014; Richardson et al., 2014; Dresing et al., 2016). Thus, magnetic connectivity is critical for identifying the dominant accelerator of SEPs.

SEP events are broadly categorized as "impulsive" or "gradual" based on their origin and particle acceleration processes. Impulsive SEP events (see Fig.6, left) are smaller in intensity and timescale, associated with short-lived X-ray flares, and characterized by enriched 3He isotopes, heavy ions, and electrons (Reames, 1999). These events show high 3He/4He ratios (up to a thousand times solar wind values) (e.g., Reames, 2013), are linked to smaller, slower, and narrower CMEs, and are confined to limited longitudes (e.g., Kahler, 1992; Reames, 2021). Impulsive SEP events rich in 3He isotopes are also associated with coronal jets occurring during magnetic reconnection (Wang et al., 2006; Raouafi et al., 2016).

Gradual SEP events (Fig. 6, right) are large, proton-rich events with gradual increases and slow decays in particle flux. They are associated with long-duration SXR flares (Oka et al., 2018), large, fast, wide CMEs, and type II radio bursts, signatures of shock-driven acceleration (Cane, 1985; Cane et al., 1988; Kahler, 1992). During gradual SEPs, shock waves from fast CMEs accelerate plasma and SEPs (e.g., Anastasiadis et al., 2019b). Abrupt SEP intensity increases during spacecraft shock crossings, as well as strong correlations between CME and large SEP event characteristics, confirm the role of CME-driven shocks in SEP acceleration (Cane et al., 1988; Kouloumvakos et al., 2019). Type II radio emissions indicate that shock-driven acceleration contributes to gradual intensity profiles and prolonged decays (Cliver and Ling, 2007). The extended duration of gradual SEP events, especially at low energies, is due to ongoing acceleration by large-scale shocks as they propagate away from the Sun (Mason et al., 1984). The SEP intensity profiles observed at different longitudes vary because the magnetic connection to different regions of the expanding shock, from the nose to the flanks or vice versa, changes over time (Cane et al.,

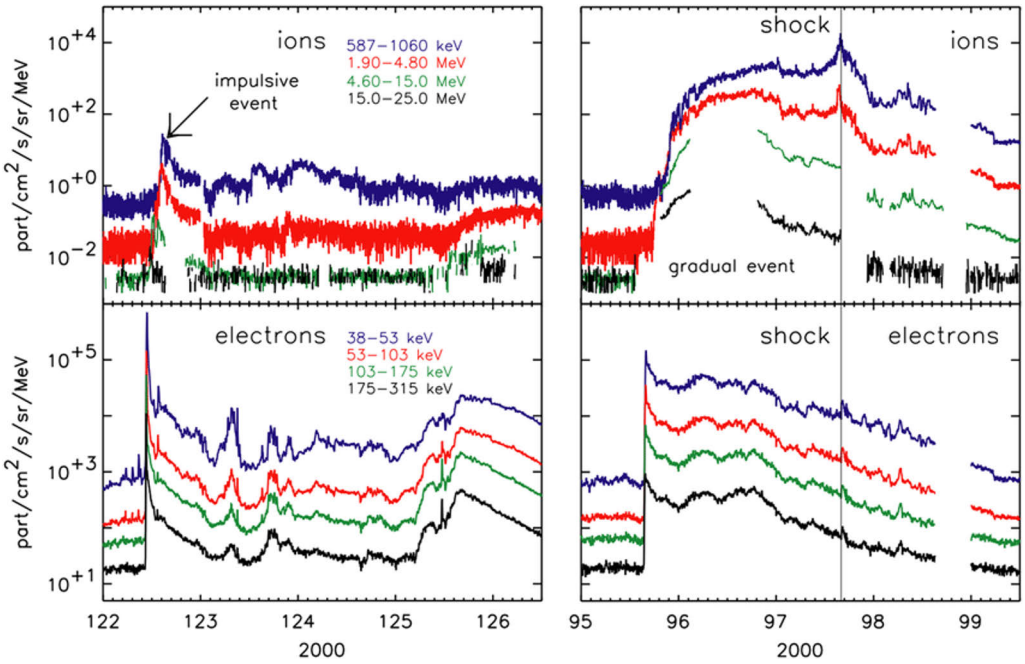

Figure 6. SEP intensity-time profiles measured by Advanced Composition Explorer (ACE), classified into impulsive (left) and gradual (right) profiles. Impulsive SEP events are associated with impulsive flare, are characterized by an impulsive time history, and are enriched with electrons and 3He isotopes. Gradual SEP events are associated with fast CME-driven shock waves, are characterized by their gradual and long-lasting flux profile, and are proton-rich. Image credit: Lario (2005), reproduced with permission from SNCSC.

1988). However, transport effects such as perpendicular diffusion, magnetic field line random walk, and particle scattering can also contribute to gradual intensity profiles and their broad distribution (e.g., Kahler, 1992).

While close to the Sun, coronal shocks also play an important role in SEP acceleration, in addition to flares. Coronal shocks, generated during solar activity in flares or accompanied by CMEs at low coronal heights (1.5–2.5 solar radii), accelerate SEPs near the Sun (Cliver et al., 2004). These shocks are generally short-lived but can become interplanetary shocks with strong, fast, and wide CMEs (e.g., Reames, 2021).

Initially, SEP events were attributed primarily to solar flares, with particle diffusion invoked to explain their wide longitudinal spread. Later, observations established CMEs and their shock waves as more effective accelerators and distributors of SEPs throughout IP space (e.g., Reames, 2021). Nevertheless, in-situ measurements from multiple spacecraft and remote sensing of solar eruptions reveal that the traditional classification into impulsive and gradual SEP events is often insufficient to describe the majority of observed events (Anastasiadis et al., 2019b).

During events when solar flares are accompanied by CME-driven shocks, it is difficult to distinguish the contributions of each mechanism to SEP acceleration (Cane et al., 2003, 2006). The dominant accelerator may also depend on the particle species and energy range. Strong correlations between proton and electron peak intensities indicate a common acceleration mechanism for both species in both well-connected and poorly-connected events (Trottet et al., 2015). In the studied sample of strong CME events, high correlations between high-energy electron peaks and coronal shock parameters suggest that shock acceleration plays a dominant role for high-energy electrons, whereas low-energy electrons may be accelerated by both flares and shocks (Dresing et al., 2022). However, the exact contributions of flares and CME-driven shocks to SEP acceleration remain an open question, complicated by their spatial and temporal association, and by complex SEP transport processes from the corona to in-situ detection near 1 au, which obscures source-specific signatures (e.g., Anastasiadis et al., 2019b; Kouloumvakos et al., 2019).

3.2 Characteristics of SEP events

SEP events have different characteristics that vary significantly between events and particle species and energies. Each of these characteristics may lead to unveiling the scientific puzzle behind the source, acceleration, and transport processes of SEPs. Elemental and isotopic abundances, along with electron-to-ion ratios observed in SEP events, provide significant information about the underlying acceleration mechanisms (e.g., Reames, 2021). The shape and slope of SEP energy spectra offer valuable insight into the potential acceleration mechanisms. Softer spectra are typically associated with flare-driven acceleration, while harder spectra suggest a dominant

contribution from shock acceleration (Lin, 1985; Klecker, 2013). The shape of electron energy spectra is characteristic of certain energies observed during a flare and is correlated with the parameters of associated X-ray emission (Moses et al., 1989).

Typical SEP time-intensity profiles consist of a rise phase, defined by the event onset, peak time, and peak intensity, followed by a decay phase. In gradual SEP events, the profiles can be more complex, especially when influenced by the passage of an IP shock at the observing spacecraft. The decay phase, during which intensity levels return to the background, can last from several hours to multiple days (Krucker et al., 2007).

The onset delay in SEPs from the associated flare or radio bursts onsets is also a useful characteristic to understand the acceleration mechanisms as shorter and longer onset delays suggest the impulsive and gradual acceleration mechanisms associated with flares and shocks, respectively. Onset delays also hint at the magnetic connectivity from the source and the corresponding transport effects for SEPs (Strauss et al., 2023). The energy dependence of SEP onset delays help to explain how SEPs are scattered during transport (Dröge, 2003).

To distinguish between the source, acceleration, and transport effects, the anisotropy (directional dependence of intensities) of SEPs is another important characteristic to study (Brüdern et al., 2018; Kollhoff et al., 2023). The anisotropic fluxes are often interpreted as signatures of SEP injection onto the magnetic field line connected to the observer, frequently associated with flares, while prolonged electron anisotropies may indicate shock-related acceleration; however, the observed anisotropy also depends strongly on existence of direct magnetic connection to the source region (Kahler et al., 2007). The variation of SEP onset delays and anisotropies with longitudinal separation of the observer from the source is found to be useful to disentangle the source effect from the SEP transport effect (Dresing et al., 2014).

In general, the shape and duration of the intensity profile of an SEP event are determined by the characteristics of the associated solar flares and CMEs, as well as by the heliocentric distance and longitudinal position of the observing spacecraft, and the SEP transport conditions (Lario et al., 2013; Haggerty and Roelof, 2002; Rodríguez-García et al., 2023b; Hyndman et al., 2025).

3.3 Multi-spacecraft in-situ observations of SEPs

In early times, in-situ analyses of SEPs were based on single-spacecraft observations of different events originating from various source regions on the Sun. These single-point measurements were sufficient to examine the variation of SEP characteristics with variation in location of solar eruption on the Sun (Cane et al., 1988). However, such observations are not sufficient to disentangle the source from particle transport effects or to determine their respective contributions along different radial and longitudinal directions from the source (Dresing et al., 2024; Hyndman et al.,

2025).

The Helios space mission, composed of twin (Helios 1, 2) spacecraft, provided significant observations about solar wind, plasma parameters, and different SEP characteristics. Observations provided by Helios proved to be a valuable contribution to build up a visual understanding of CMEs during its closer flyby to the Sun (Webb and Jackson, 1990). With Helios 2 observations reaching as close as 0.30 au to the Sun, researchers were able to better understand variations in the solar wind and magnetic field structures at different locations (Grappin et al., 1990; Cane and Reames, 1990). However, Helios were limited to ecliptic plane only and were unable to observe any latitudinal variations in SEP characteristics. In addition, due to the lack of imaging instruments and EUV observations, Helios was not able to provide any corona-graphic observations, even during its flyby close to the Sun, and the source locations of many backside events remained unclear.

The two STEREO (A, B) spacecraft, combined with near-Earth missions like SOHO, Wind, and ACE, offered a valuable platform for studying SEP events across a wide longitudinal span over an extended period. Still, their similar heliocentric location limited the ability to assess radial dependencies (Dröge et al., 2016).

Hence, limited spatial coverage from two or three spacecraft remains insufficient to disentangle SEP source and transport effects or to determine whether variations in SEP profiles arise from radial or longitudinal separations between observers (Hyndman et al., 2025).

Therefore, multi-point observations of the same SEP event, captured from spacecraft widely separated in both radial and longitudinal directions, are crucial for investigating the influence of the source, particle transport mechanisms, and the overall angular and spatial extent of the event (Wibberenz and Cane, 2006). Multi-point observations also reduce the influence of event-to-event variability and increase the likelihood of detecting solar eruptions more frequently, thereby providing a richer dataset for analyzing SEP events (Rodríguez-García, 2024).

With the beginning of solar cycle 25, significant progress has been made in expanding the number of in-situ observers positioned at various locations around the Sun. The addition of new space missions such as Solar Orbiter (Müller et al., 2020) and Parker Solar Probe (PSP) (Fox et al., 2016) represents a major advancement in the multi-spacecraft solar observation network. When combined with long-standing missions like SOHO (Domingo et al., 1995), Wind (Ogilvie and Desch, 1997; Wilson et al., 2021), and STEREO A, as well as the BepiColombo mission en route to Mercury (Benkhoff et al., 2021), this constellation of spacecraft constitutes an unprecedented fleet for comprehensive in-situ observation of the heliosphere (Dresing et al., 2024).

Observations from radially aligned spacecraft help characterize CME-driven shock propagation and the variation of magnetic field structures and plasma parameters across the sheath region, as well as changes in the solar wind structure during shock

crossings (Kilpua et al., 2021; Trotta et al., 2023, 2024). Multi-spacecraft observations of SEP events at different longitudes provide estimates of their angular spread, offering insight into the strength and nature of the source. Measurements of SEPs, solar wind, and plasma parameters at multiple locations enable studies of particle velocities and travel times, improving our understanding of particle injection, source characteristics, and transport processes (Rodríguez-García et al., 2025).

In-situ observations by spacecraft separated radially but located within narrow longitudinal sectors have proven useful for examining the radial dependence of particle diffusion and for highlighting the role of large-scale IP magnetic structures, such as stream interaction regions, in shaping SEP characteristics, in addition to CMEs (Rodríguez-García et al., 2023a; Kollhoff et al., 2023; Lario et al., 2022). Large, widespread eruptions observed by the current multi-spacecraft fleet distributed around the Sun allow the evolution of CMEs and their associated shocks to be tracked at multiple locations. Comparing SEP injection times, flare timings, and shock crossings at different observers helps identify distinct sources for electrons and protons and assess whether widespread SEP events result from extended sources or IP transport effects (Dresing et al., 2023). Such multi-view observations, including events studied by Dresing et al. (2025) with six spacecraft distributed around the Sun, demonstrate how a single eruption can drive a widespread shock extending to distant magnetic connections (Dresing et al., 2025).

Thus, multi-spacecraft observations are providing more comprehensive visualization of the coronal and IP environments and making it possible to better understand the dynamic processes related to the source and acceleration mechanisms of SEPs, while also helping to disentangle source-related effects from those arising during IP transport (Dresing et al., 2024).

4 Data Selection and Analysis Methods

In this chapter, we describe the data and methodology used for the analyses performed in this thesis, following the order of **Paper I, II, and III**. We introduce the SERPENTINE (Solar EneRgetic ParticlE aNalysis plaTform for the INner hEliosphere) SEP event catalog, the major data base for this thesis, and explain the content for the establishment (**Paper I**) and extension of the catalog. We provide the details of multi-spacecraft observations of SEP events of different particle species and energies, and the analyses methods used to examine the data, to study the correlation of peak intensities (**Paper II**), and the average intensity-time profiles of SEPs based on superposed epoch analysis (**Paper III**).

4.1 SERPENTINE SEP event catalog for solar cycle 25

During the initial phase of the study, a significant contribution was made as a co-author towards the compilation of an SEP event catalog (Dresing et al., 2024) within the scope of the SERPENTINE project. The SERPENTINE SEP event catalog for solar cycle 25 was established to report the multi-spacecraft observations of energetic SEP events from early solar cycle 25, containing data from November 2020 to May 2023 and is available at `https://doi.org/10.5281/zenodo.10732268`. The selection criterion for an SEP event in the catalog is that a proton event must be observed at 25–40 MeV energy by at least two different spacecraft. In the SERPENTINE SEP event catalog, SEP event parameters such as onset time, peak time, and peak intensities, as well as associated flares and type II radio bursts, are reported. This information is compiled for SEP events for $\geq$25 MeV protons, $\sim$100 keV and $\sim$1 MeV electrons, including data from multiple missions: Solar Orbiter (Müller et al., 2020), STEREO A (Kaiser et al., 2008), SOHO (Domingo et al., 1995), Wind (Ogilvie and Desch, 1997; Wilson et al., 2021), the BepiColombo (Benkhoff et al., 2021), and PSP (Fox et al., 2016). The instruments aboard different spacecraft used for the observations include: Solar Orbiter/ Energetic Particle Detector (EPD) (Rodríguez-Pacheco et al., 2020), STEREO / Solar Electron Proton Telescope (SEPT) (Müller-Mellin et al., 2008), STEREO / High Energy Telescope (HET) (von Rosenvinge et al., 2008), Wind / Three-Dimensional Plasma and Energetic Particle Investigation (3DP) (Lin et al., 1995), SOHO/ Energetic and Relativistic Nuclei and Electron-Heavy ion Detector (ERNE-HED) (Torsti et al., 1995), SOHO / Elec-

Table 1. Details of the instruments aboard different spacecraft utilized for the multi-spacecraft observations of the SERPENTINE SEP event catalog.

Spacecraft / Instrument	Energy range (MeV)		Detection principle
	Electrons	Protons	
SOHO / ERNE / HED	–	13 – 130	$\mathrm{d}E/\mathrm{d}x$–E[a]
SOHO / EPHIN	0.25 – 10.4	4.3 – 53	$\mathrm{d}E/\mathrm{d}x$–E
Wind / 3DP	0.02 – 0.67	0.06 – 8.78	magnet[b]/foil[c]–E
STEREO / HET	0.70 – 4	13.6 – 60	$\mathrm{d}E/\mathrm{d}x$–E
STEREO / SEPT	0.04 – 0.42	0.08 – 6.50	magnet/foil–E
Solar Orbiter / EPD / HET	0.45 – 18.83	7.04 – 104.90	$\mathrm{d}E/\mathrm{d}x$–E
Solar Orbiter / EPD / EPT	0.03 – 0.47	0.055 – 6.13	magnet/foil–E
PSP / EPI-Hi / HET	0.4 – 11.3	6.70 – 90.50	$\mathrm{d}E/\mathrm{d}x$–E
PSP / EPI-Lo	0.01 – 9.96	0.07 – 8.73	Time-of-flight[d]–E
BepiColombo / SIXS-P	0.07 – 6.46	1.12 – 50.71	foil–E, $\mathrm{d}E/\mathrm{d}x$–E

[a] $\mathrm{d}E/\mathrm{d}x$–E technique separates species utilising an energy-loss signal ($\mathrm{d}E/\mathrm{d}x$) from a transmission detector above the stopping detector measuring the residual energy (E).
[b] A magnet is used to deflect electrons while passing ions into the detector measuring the energy (E).
[c] A foil is used to stop low energy protons while passing electrons into the detector measuring the energy (E).
[d] Time-of-flight measurement determines the speed of the particle, which combined with energy (E) can determine the mass of the particle, allowing the detector to distinguish between particles.

tron Proton Helium Instrument (EPHIN) (Müller-Mellin et al., 1995), PSP / Energetic Particle Instrument High energy telescope (EPI-Hi) and PSP/ Energetic Particle Instrument Low energy telescope (EPI-Lo) (McComas et al., 2016), and Bepi-Colombo / Solar Intensity X-Ray Particle Spectrometer-Particle instrument (SIXS-P) (Huovelin et al., 2020) . The details of energy ranges and the particle detection principles for instruments abroad different spacecraft for electrons and protons are provided in Table 1. Another important parameter calculated is the peak intensity ratio for $\sim$1 MeV electrons to $\geq$25 MeV protons for all spacecraft observations (for details, see Sect. 4.1.3).

The information utilized for this thesis on the associated CMEs, including their projected linear speeds and angular width, is taken directly from the SERPENTINE-CME list[1], based on the Coordinated Data Analysis Workshops (CDAW) SOHO-LASCO CME catalog[2]. The SERPENTINE-CME list provides information on multiple CMEs in the time scale of the SEP event. However, we limit our selection to the CMEs reported to be the fastest and most likely associated with the respective SEP

[1] `https://data.serpentine-h2020.eu/catalogs/cme/`
[2] `https://cdaw.gsfc.nasa.gov/CME_list/`

event (**Paper II**).

The SERPENTINE SEP event catalog contains information on metric and DM type II radio bursts, based on radio spectrograms from PSP, STEREO A, Solar Orbiter, and Wind, along with ground-based observations. We limited our use, following Cliver and Ling (2007), only to the DM type II radio burst information in this thesis (**Paper II**).

4.1.1 Databases used for flare association

The flare identification in the SERPENTINE SEP event catalog is mainly based on the GOES observations from Solar-monitor.org, Hinode satellite, and the Space Weather Prediction Center (SWPC) (Dresing et al., 2024). These sources utilize only Earth-based or near-Earth-based observations. Since the orbit of Solar Orbiter is different from that of Earth, it can sometimes observe the far side of the Sun, which is not visible from Earth. As a part of this study (**Paper I**), Solar Orbiter/Spectrometer Telescope for Imaging X-rays (STIX) observations[3] are used to identify the flare in a few cases where the flare was behind the limb as seen from Earth. Among the 45 SEP events of the catalog, five events where the flare was not on the visible disc as seen from Earth or Solar Orbiter are left with missing flare identification. Further details on flare identification using Solar Orbiter/(STIX) observations are provided in Sect. 4.1.4.

4.1.2 Onset and peak determination

As a part of this study (**Paper I**), the SEP intensity-time profiles of the sample are analyzed to determine the onset time, the peak time, and the peak intensity using the onset determination tool of the SERPENTINE project (Palmroos et al., 2022), based on the Poisson-CUSUM (cumulative sum) method (Lucas, 1985; Huttunen-Heikinmaa et al., 2005). The CUSUM method monitors the variations in intensity-time series and indicates the time stamp as the onset of the event when the CUSUM starts to increase above a certain threshold level. We report the onset time, peak time, and peak intensity for each spacecraft observation of the SEP events, defining the peak of the event as the global intensity maximum (Fig. 7). The information about the time averaging used for onset and peak determination, as well as the viewing direction of the observation, is also provided in the catalog. In cases where instruments have multiple viewing directions for onset and peak determination, we used the direction resulting in the earliest onset and highest peak intensity, respectively. If no onset is detected by a certain spacecraft, the background intensity is still reported during the period of the event observed by other spacecraft. The catalog also provides the inferred injection

[3] `https://github.com/hayesla/stix_flarelist_science`

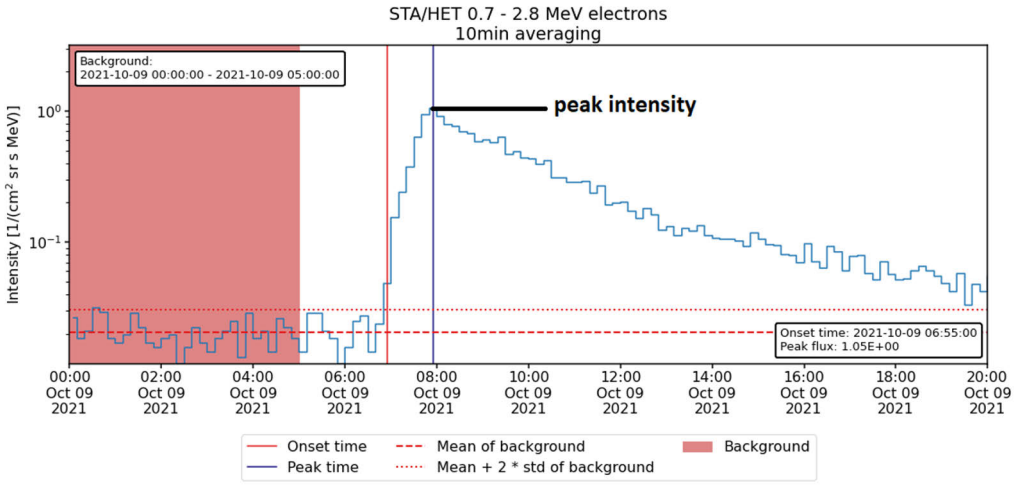

Figure 7. Onset and peak determination of an example SEP event using the onset determination tool (Palmroos et al., 2022). The blue curve represents the intensity-time series of the SEP event, with the red shaded region representing the event background. The red and violet vertical lines indicate the onset and peak times, with the corresponding peak intensity, respectively.

times for all SEPs using the time shift analysis (Paassilta et al., 2018), which shifts the onset back in time to the Sun, depending upon the travel time of SEPs from the Sun to the observer. The estimated path length traveled by SEPs along a nominal Parker spiral and the solar wind speed used for these calculations are also provided in the catalog. The solar wind speed is measured at the onset time at the observer while, if speed measurement is not available, a nominal speed of 400 km s^{-1} is used.

The peak intensities of $\geq$25 MeV protons and $\sim$100 keV electrons used in this thesis (**Paper II**) are taken directly from the SERPENTINE SEP event catalog. The peak intensities of $\sim$1 MeV electrons are calculated using interpolation and sometimes an extrapolation technique applied between measurements from two different instruments, as explained in Sect. 4.1.3. The peak intensities of $\sim$1 MeV electrons calculated in this way are used to report the ratio of peak intensities of $\sim$1 MeV electrons to $\geq$ 25 MeV protons in the SEP event catalog as well.

4.1.3 Determination of particle intensities at comparable energies across different spacecraft instrumentation

The ratio of high-energy electron to proton peak intensities is an important parameter for studying the potential contribution of different sources towards the acceleration of SEPs (Cliver and Ling, 2007; Cane et al., 2010; Farwa et al., 2025a). For this purpose, the ratio of peak intensities of $\sim$1 MeV electrons to $\geq$25 MeV protons is calculated and reported in the SERPENTINE SEP event catalog. If the mean energy

of a single channel does not match the desired energy level, certain energy channels are combined to calculate the effective energy as a geometric mean of the limits of the combined channels. The instruments, energy channels, and the corresponding effective energies (in case of combination of channels) used for the peak intensities reported in the catalog are given in Table 1 of Dresing et al. (2024). For $\geq$25 MeV protons, the effective energies from different instruments mostly agree on a single value (32 MeV), which is not the case for $\sim$1 MeV electrons, due to unavailability of possible matching energy channels (Table 1 of Dresing et al. (2024)). In the case of $\sim$1 MeV electrons, the best possible energy match is readily obtained from the first channel of STEREO/HET, with an effective energy of 0.99 MeV. Therefore, the peak intensities of $\sim$1 MeV electrons from other spacecraft instruments are calculated at 0.99 MeV separately (**Paper I**) based on an interpolation (sometimes extrapolation) technique applied between measurements from two different instruments. To achieve the best possible energy match of 0.99 MeV for electrons, the energy channels and corresponding effective energies used to calculate the electron-to-proton peak intensity ratio for different spacecraft are given in Table 2 of Dresing et al. (2024).

We applied the logarithmic interpolation/extrapolation technique on the energy spectra from different instruments. For example, in the case of the Solar Orbiter, the best possible energy match of 0.99 MeV is situated between the energy ranges covered by the EPT and HET instruments. We, therefore, utilized measurements from both these instruments to calculate the $\sim$1 MeV peak intensity. We applied the interpolation, based on a power law, between intensity measurements for channel 1 of HET and a combined energy channel of channels 31–33 for EPT. If the event was not observed in the HET, we extrapolated the EPT measurement using an average slope determined from the events with observations at both instruments.

4.1.4 SOLER SEP event catalog for solar cycle 25

SERPENTINE SEP event catalog for solar cycle 25 is recently extended, within the scope of the Energetic Solar Eruptions: Data and Analysis Tools (SOLER) project, as the SOLER SEP catalog, available at `https://soler-eu.streamlit.app/`. The author of the thesis has extended the SEP event analysis for the SOLER catalog to 98 independent events in total, from November 2020 to December 2023. The SOLER SEP event catalog is based on the data from same set of six spacecraft, providing measurements for $\geq$25 MeV protons, $\sim$100 keV and $\sim$1 MeV electrons. The selection criterion for an SEP event for SOLER catalog, is that a proton event must be observed at 25–40 MeV energy by at least one spacecraft, which is different from the SERPENTINE catalog where an SEP event must be observed by at least two different spacecraft. With this selection criterion, 20 new SEP events are included within the timeline of the SERPENTINE catalog, while 33 new SEP events are included from May 2023 to December 2023. All the SEP event parameters described in Sect. 4.1

are provided for the extended catalog as well, with onset determination performed using the PyOnset tool of the SOLER project, based on a Poisson-CUSUM bootstrap hybrid method (Palmroos et al., 2025). This method combines the Poisson-CUSUM (Lucas, 1985; Huttunen-Heikinmaa et al., 2005) method with statistical bootstrapping of the background of SEP event observations, and provides more accurate onset times along with their uncertainties. The onset times provided in SERPENTINE catalog are also revised with this improved onset determination method. The author performed the flare association for new events based on identification from the SOLER flare catalog, available at `https://soler-eu.streamlit.app/`, enlisting STIX and GOES flares with class $\geq$ M5. For an event where no flare is reported in the SOLER flare catalog, the flare association is performed using the same sources as for the SERPENTINE catalog (for details, see Sect. 4.1). The most likely flare candidate is associated based on a possible match between the SEP and flare onset times, and a suitable flare location corresponding to the longitude of the spacecraft observing the earliest SEP onset. The author also performed the CME association for the SEP events from the SOLER CME catalog, available at `https://soler-eu.streamlit.app/`, which enlists fast CMEs with speed $\geq$ 1000 km s^{-1}, and is based on the SOHO/LASCO CME catalog. For CME association, we looked into LASCO movies within the time window of 2–3 hours after the earliest SEP onset, and identified the most likely CME candidate based on matching the inferred position of CME origin with the location of the flare associated with the event. We note that, at the time of our analysis, PSP electron data were available publicly only in the form of count rates, and, as an exception, we were provided with the electron intensity data within the SERPENTINE project. Hence, for the new events included in the SOLER SEP event catalog, the PSP electron ($\sim$100 keV and $\sim$1 MeV) measurements are reported in count rates instead of peak intensities. A conversion factor is calculated to estimate PSP electron peak intensities from the count rates, based on a linear model with slope of 1, fitted to the data points of logarithmic electron peak intensities and the logarithmic count rates for the events from the SERPENTINE SEP event catalog (Fig. 8). Hence, the conversion factor is calculated as $10^{(c\pm\Delta C)}$, where c and ΔC are the values of the y-intercept, and the uncertainty in the y-intercept, respectively, of the linear fits (Fig. 8). The values of c and ΔC calculated for $\sim$100 keV electrons are 3.52 and 0.015, respectively, and for $\sim$1 MeV electrons are 1.70 and 0.040, respectively. By using the PSP electron scaling factors, the proxies for $\sim$100 keV and $\sim$1 MeV electrons peak intensities are provided in the SOLER SEP event catalog.

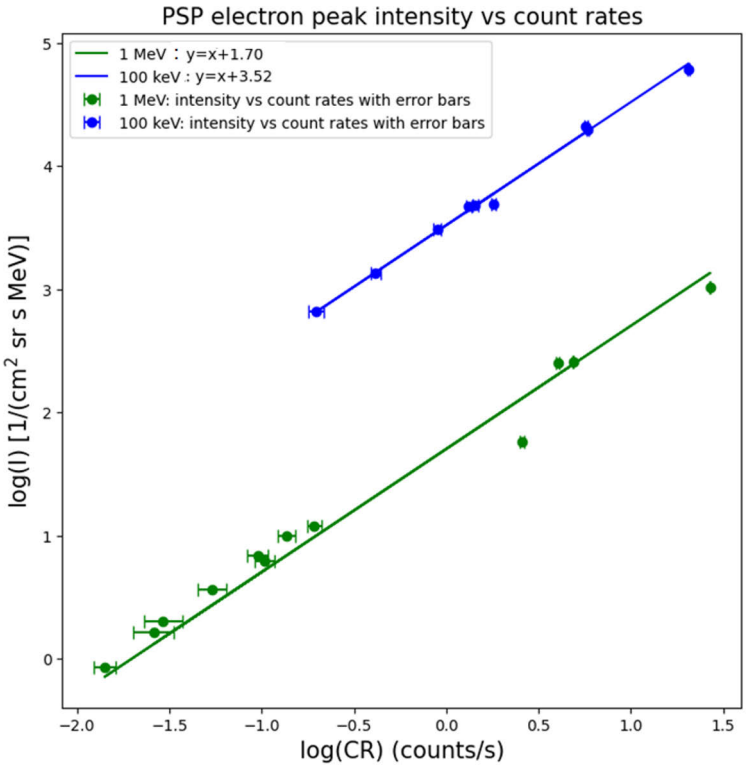

Figure 8. A linear model (slope=1) is fitted to the logarithmic peak intensities and logarithmic count rates for ∼1 MeV (green) and ∼100 keV (blue) electrons.

4.2 Calculation of correlation of the SEP event parameters

Studying correlations between various parameters of SEP events and their solar sources has significantly advanced our understanding of SEP characteristics, and the underlying acceleration and transport processes (Cane, 1985; Cliver and Ling, 2007; Richardson et al., 2014; Dresing et al., 2014, 2022; Rodríguez-García et al., 2023a). For example, correlations between SEP intensity and CME speed or X-ray flare intensity help distinguish whether shocks or flares serve as the primary source of SEPs, (Kahler, 2001), while the relationship between longitudinal spread and SEP peak intensities sheds light on potential transport mechanisms (Lario et al., 2013). Analyzing correlations among SEP parameters also facilitates event classification, (e.g., Reames and Stone, 1986), and comparing the peak intensities of relativistic electrons and high-energy protons has enabled the development of empirical forecasting models (Posner, 2007).

In this study (**Paper II**), we examined the correlation between different SEP event parameters and their dependence on the magnetic connection (for details, see Sect. 4.2.3) of the observer from the source region. The following methods are applied to the dataset to make the measured peak intensities compatible for correlation analysis.

4.2.1 Instrumental inter-calibration

Different instruments measuring SEPs aboard different spacecraft, have varying sensitivities, energy responses, resolutions, and measurement techniques, leading to possible mismatches and discrepancies in the data. Degradation of an instrument due to aging and saturation effects under high fluxes may also reduce the reliability of the results. Inter-calibration of different instruments is essential to standardize all measurements of a certain parameter for accurate comparison of measurements from different sources, thus improving the reliability of scientific interpretation of the data. To make the multi-spacecraft SEP observations consistent, different inter-calibrations were applied across STEREO/HET A versus B, STEREO/HET versus SOHO/ERNE (Richardson et al., 2014), STEREO/SEPT versus ACE/EPAM, and STEREO/HET versus GOES/EPS and SOHO/COSTEP/EPHIN (Lario et al., 2013).

In this study (**Paper II**) the STEREO A/HET measurements are inter-calibrated with Solar Orbiter/HET, and then a scaling factor is applied to the PSP measurements to calibrate them to STEREO/HET (for details, see appendix B **Paper II**). The $\sim$1 MeV electron peak intensities measured by STEREO A/HET are found to be systematically low compared to the Solar Orbiter/HET measurements (Farwa et al., 2025a). The $\sim$100 keV electron peak intensities measured by STEREO A/SEPT and Solar Orbiter/EPT are on a common baseline, which is used for an inter-calibration

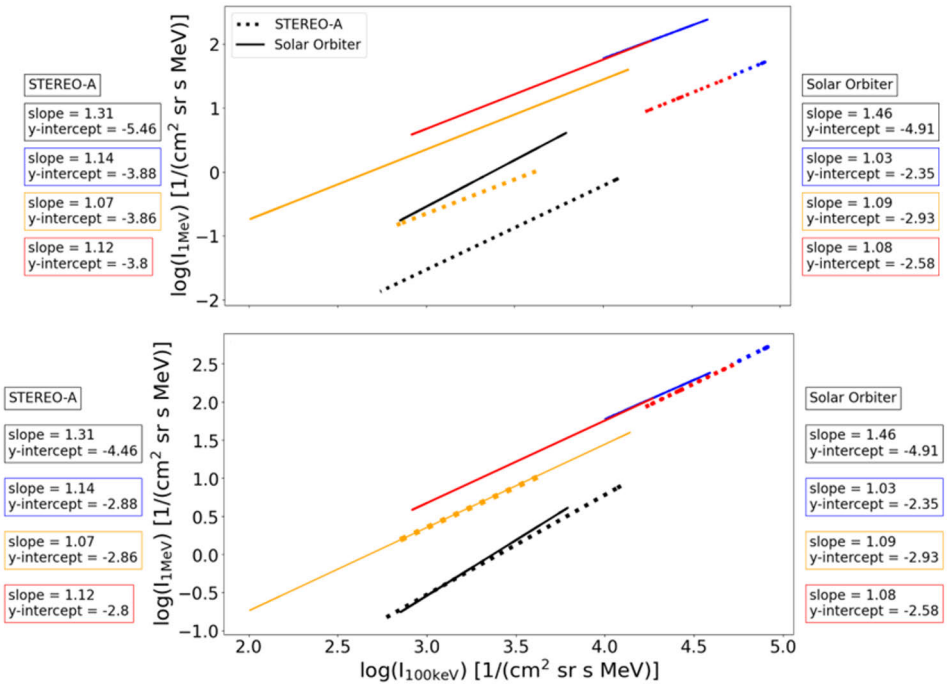

Figure 9. Calculation of the inter-calibration factor for STEREO A/HET. The upper panel shows the linear fits applied to intensity profiles of four events (different colors) observed by STEREO A (dotted lines) and Solar Orbiter (solid lines). The lower panel shows the alignment of STEREO A fits to those of Solar Orbiter. The value of slope and y-intercept for each fit for different events are provided in legend boxes of the corresponding colors. Image credit Farwa et al. (2025a), reproduced and licensed under CC BY.

between the STEREO A/HET and Solar Orbiter data. Intensity profiles of the decay phase, being near isotropic, are selected for ∼1 MeV and ∼100 keV electrons for some events simultaneously observed by both instruments (STEREO/SEPT and Solar Orbiter/EPT), and are fitted linearly (Fig. 9, upper panel). To inter-calibrate the HET measurements, a best possible alignment is obtained by raising all STEREO fits to Solar Orbiter data values (Fig. 9, lower panel) by adding 1 to the STEREO fit's logarithmic y-intercepts, resulting in an inter-calibration factor of $10^1 = 10$ for STEREO A/HET measurements. Our calculation is in good agreement with the inter-calibration factor of ∼15 between STEREO/HET and SOHO/EPHIN reported by Lario et al. (2013) and Richardson et al. (2014).

The PSP electron measurements are inter-calibrated by applying a constant factor to PSP intensities to level them up to the same baseline as the STEREO A (and Solar Orbiter) measurements (for details, see Appendix B, **Paper II**). The STEREO A and PSP measurements for ∼1 MeV (Fig. 10, upper panel) and ∼100 keV (Fig. 10, lower panel) electron peak intensities as a function of ∼25 MeV proton peak intensities are studied. The electron-to-proton peak intensities vary similarly for both spacecraft observations with PSP electron observations being systematically lower than those of STEREO A observations for a given ∼25 MeV proton peak intensity (Fig. 10, left panel). To level the PSP observations to the same baseline as STEREO A, a best-fit multiplier is applied to PSP observations by calculating a factor C^{PSP} to bring the PSP data set into the best possible agreement with the level obtained by fitting electron peak intensities versus proton peak intensities for STEREO A (Fig. 10, right panel).

The value of C^{PSP} is calculated by minimizing

$$\chi^2 = \sum_{i=1}^{N^{\mathrm{PSP}}} [\log I_{\mathrm{e},i}^{\mathrm{PSP}} + \log C^{\mathrm{PSP}} - (a^{\mathrm{STA}} + b^{\mathrm{STA}} \log I_{\mathrm{p},i}^{\mathrm{PSP}})]^2, \tag{1}$$

where a^{STA} and b^{STA} represent the values of intercept and slope parameters obtained from the fit applied to the STEREO A observations (Fig. 10, left panel), and the sum is taken over all PSP observations.

The re-normalization factor obtained for the ∼100 keV and ∼1 MeV electrons channels is $C^{\mathrm{PSP}}_{100\,\mathrm{keV}} = 3.069$, and $C^{\mathrm{PSP}}_{1\,\mathrm{MeV}} = 3.84$, respectively, bringing the PSP electron (purple plus markers) onto a common baseline with STEREO A (Fig. 10, right panel).

4.2.2 Radial scaling

The heliocentric location of the observing spacecraft affects the measured peak intensities of SEPs. At larger radial distances, the SEPs occupy a larger volume, and due to the ongoing scattering and diffusion of the particles ejected from the Sun, the

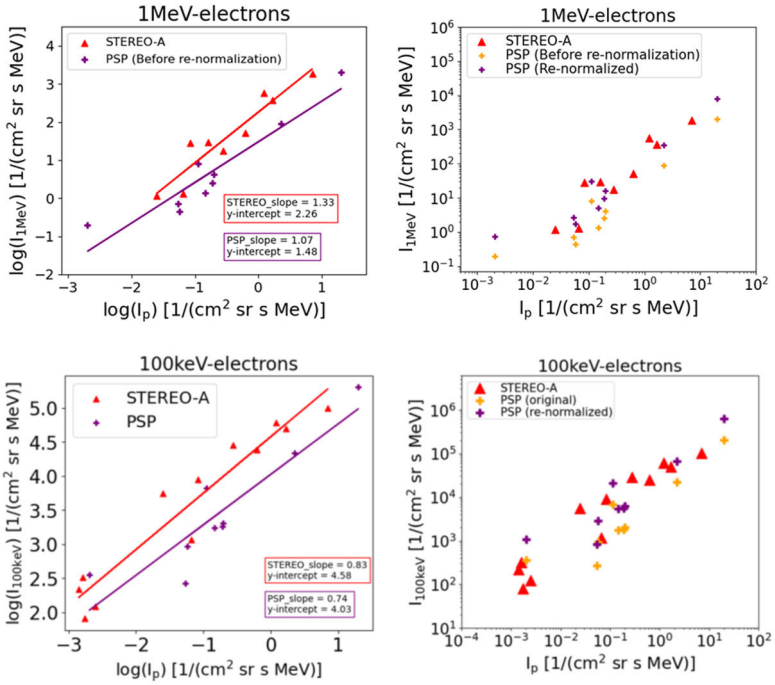

Figure 10. Calculation of the PSP re-normalization factor for ∼1 MeV (top panel) (Farwa et al., 2025b) and ∼100 keV (bottom panel) electrons (Farwa et al., 2025a). The left panel displays the linear fits applied to both STEREO A and PSP data points, while the right panel presents the results of the PSP re-normalization applied to the electron measurements. In the right panel, orange and purple plus markers indicate the PSP measurements before and after re-normalization, respectively. Image credit: Farwa et al. (2025b,a) , reproduced and licensed under CC BY.

intensity of SEPs decreases as these particles travel away from the Sun (Lario et al., 2006; Dayeh et al., 2010; Lario et al., 2013; Rodríguez-García et al., 2023b). Hence, the peak intensities measured at different heliocentric distances R cannot be used to compare peak intensities of different species or for studying the correlations of peak intensities with different SEP parameters. In order to make all the measurements comparable, it is required to radially scale all spacecraft observations to a certain radial distance. The radial dependence of SEP peak intensities is assumed to vary as $R^{-\alpha}$ where the value of α depends on the particle species and energy, and may also vary from event to event. A value of α is reported as 2.7 and 1.9 for 4–13 MeV and 27–37 MeV protons, respectively (Lario et al., 2006), and as $\sim$3 for 71–112 keV electrons (Lario et al., 2013). In a recent study, Rodríguez-García et al. (2023b), taking into account the possible uncertainties, concluded that for near-relativistic electrons, the radial dependence of SEP peak intensity varies as R^{-3}.

During the time frame of the SERPENTINE SEP event catalog, the observing spacecraft were located at different R ranging in 0.07–1.01 au. A radial scaling is applied to all spacecraft observations (**Paper II**), and peak intensities are corrected by scaling all the measurements taken at different R to a distance of 1 au, as $I_{\text{corrected}} = I_{\text{observed}} R^{\alpha}$, where $\alpha = a \pm b$, with a as the scaling factor and b as a measure of uncertainty in the value of α. The values of these scaling factors for both electron energies are used as reported by Rodríguez-García et al. (2023b) for near-relativistic electrons and by Lario et al. (2006) for 27–37 MeV protons.

4.2.3 Longitudinal classification of SEP events

Magnetic field geometry, plasma parameters, and solar wind conditions vary along the Parker spiral at different longitudes, affecting SEP propagation. However, the dominant factor governing the variation in SEP observations at different locations is the longitudinal distance from the source region, with peak intensities generally decreasing as the longitudinal separation from the eruption center increases. Consequently, observers at different longitudes record distinct SEP profiles and peak intensities for the same event.

The longitudinal classification of SEP events is helpful to distinguish between the source mechanisms and the transport effects, provided that the transport conditions do not vary significantly between observers (Cane et al., 1988; Dresing et al., 2012; Richardson et al., 2014; Dresing et al., 2014), and to understand the variation of SEP characteristics over the longitudinal spread of the event (Cane et al., 1988; Cliver and Ling, 2007; Lario et al., 2013; Núñez, 2018; Rodríguez-García et al., 2023b).

The magnetic connection between an observer and the Sun is estimated by back-mapping the Parker spiral from the observer to its solar footpoint, with the type of this connectivity determined by the longitudinal separation between the footpoint and the source location. Figure 11 provides an explanation of the longitudinal classi-

fication of SEP events used in this study, based on the magnetic connectivity between the observer and the source by displaying the positions of different spacecraft during an example event. This interpretation is based on the idealized Parker spiral model of the IP magnetic field; however, deviations from this configuration can occur in reality owing to solar wind inhomogeneities, transient structures, and magnetic field distortions. The black dashed spiral (Fig. 11) represents the magnetic field line connecting to the flare location, while the black arrow indicates the flare longitude. The numbers and colors on the spiral curves denote the field lines connecting to each spacecraft. Each sector—green, orange, and pink—indicates whether a spacecraft is well-connected to the event, poorly-connected with the flare to the west of the field line footpoint (sector of western events), or poorly-connected with the flare to the east of the footpoint (sector of eastern events). Following the convention of Cliver and Ling (2007), we defined a "well-connected" event as one in which the observing spacecraft has a longitudinal separation of $-35^\circ \leq \Delta\Phi \leq 35^\circ$ from the flare location. In contrast, "poorly-connected" events are those where the magnetic connection lies outside this range, further categorized into western events where $35^\circ \leq \Delta\Phi \leq 180^\circ$, and a sector of eastern events, where $-180^\circ \leq \Delta\Phi \leq -35^\circ$. The Solar-MACH tool (Gieseler et al., 2023) uses ballistic back-mapping to determine these longitudes, as reported in the SERPENTINE catalog.

The magnetic connection of an observer to the source flare is calculated as the longitudinal separation angle, $\Delta\Phi$, defined by Lario et al. (2013) as in Eq. (2)

$$\Delta\Phi = \Phi_{\mathrm{flare}} - \Phi_{\mathrm{SC}} \tag{2}$$

where Φ_{flare} is the longitude of the flare and Φ_{SC} is the longitude of the spacecraft magnetic footpoint, measured in the Carrington coordinate system. Magnetic connection is typically quantified by the longitudinal separation between the source region and the observer, since longitudinal separation has been found to be the main parameter affecting SEP intensity and timing (Stansby et al., 2021). Most of the spacecraft orbit in the ecliptic plane, minimizing the latitudinal separation of the observer from the source, even though total angular separation could, in principle, also be used. Thus, longitudinal separation is most commonly used to describe whether a spacecraft is magnetically connected to a flare.

4.2.4 Calculation of correlation coefficients

There are different statistical techniques that are used to calculate the correlation between different parameters, such as SEP peak intensities, spectral characteristics, onset delays, flare intensity, CME speeds and angular width, and longitudinal spread of the event (Cane, 1985; Cliver and Ling, 2007; Richardson et al., 2014; Trottet et al., 2014; Ravishankar and Michalek, 2021; Rodríguez-García et al., 2023a).

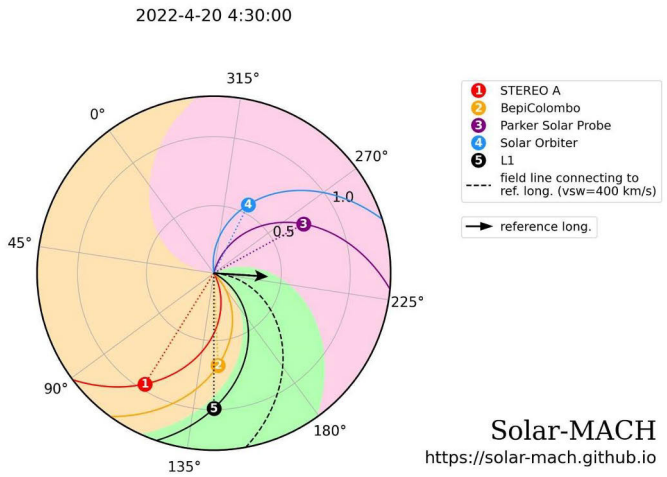

Figure 11. An example SEP event observed by multi-spacecraft with different longitudinal configurations (Farwa et al., 2025a). With reference to the flare longitude, the events observed by the corresponding observers are divided into well-connected (green), poorly-connected western (orange), and poorly-connected eastern (pink) events. Depending on the longitudinal separation, L1 (black) observes well-connected, and PSP (purple), and Solar Orbiter (blue) observe poorly-connected eastern events. While the STEREO A (red) and BepiColombo (orange) observe poorly-connected western events. Image credit: Farwa et al. (2025a) , reproduced and licensed under CC BY.

The correlation coefficient (CC) is a measure of the strength of the relationship between two variables, and it gives an estimate of how strongly the variation of one variable affects the value of the other variable (Rodgers and Nicewander, 1988; Spearman, 1904). CCs calculated to examine the correlations between different variables, include the Pearson correlation coefficient (PCC) and the Spearman correlation coefficient (SCC). PCCs are calculated to investigate the correlation between two variables having a linear relation in a continuous data set with a normal distribution. PCCs are more sensitive to outlier points in the data set, and this method cannot differentiate between dependent and independent variables. SCCs, on the other hand, are calculated for variables having a monotonic relation, are less sensitive to outlier points, and can be calculated for both continuous and discrete data sets (Spearman, 1987).

In this thesis (**Paper II**) the correlations are studied between the electron and proton peak intensities, between SEP peak intensities and the intensity of the associated X-ray flare, and the CME speed. Based on the statistical advantage of the SCC method over the PCC method described above, SCCs, represented as ρ in Eq. (3) are calculated between different SEP and source parameters in the present study (**Paper II**).

$$\rho = 1 - \frac{6 \sum_{i=1}^{n} d_i^2}{n(n^2 - 1)} \tag{3}$$

where n is the total number of data points, and d_i is the difference between the ranks of both variables. ρ has values between -1 and +1, with value -1 (+1) representing the negative (positive) correlation between the variables implying that an increase in one variable will result in a decrease (increase) in other variable. ρ with a value 0 represents no correlation at all.

The strength of each correlation is assessed using the absolute value of ρ, with $\rho > 0.5$ indicating a stronger correlation and $\rho < 0.5$ indicating a weaker one. Statistical significance is evaluated using the p-value, which tests the likelihood of observing such a correlation by chance under the null hypothesis of no real correlation. A statistically significant correlation is indicated by a lower p-value, whereas a higher p-value denotes a non-significant result (Spearman, 1987). Correlations with p-values less than 0.05 are considered statistically significant in this thesis (**Paper II**).

Apart from the calculation of CCs used in this thesis, different methods have been used by other researchers to study the correlations between SEPs and source parameters. These methods include linear regression (Ravishankar and Michalek, 2021), Bayesian regression (Rodríguez-García et al., 2023a) and the Pearson and partial correlation technique (Trottet et al., 2014; Samwel and Miteva, 2023; Miteva et al., 2024).

4.3 Superposed epoch analysis of SEP profiles

Based on characteristic shapes for certain energies and particle species, SEP intensity profiles contain key information about the source, acceleration, and transport processes of SEPs (Cane, 1985; Cane et al., 1988; Kecskemety et al., 2009; Dresing et al., 2014; Richardson et al., 2014). Similarities in intensity-time profiles of relativistic electrons and high-energy protons provides grounds for space-weather forecasting models against SEP radiation hazards (Posner, 2007).

Superposed epoch analysis (SEA) is a valuable technique for investigating the average behaviour of SEP profiles, solar wind and plasma parameters, and different magnetic structures (Prikryl et al., 2014; Masías-Meza et al., 2016). Recently, SEA has been applied to SEP intensities to obtain an average SEP profile and to investigate the role of shock acceleration for electrons and protons (Kartavykh et al., 2025).

SEA is a powerful statistical tool in data analysis used to identify temporal changes and distinct patterns in a dataset relative to specific times or events, known as epochs. It is typically employed to describe the average behavior of data over these epochs by defining a time window around each selected epoch. The data, usually comprising a series of events related to some physical phenomenon, are then

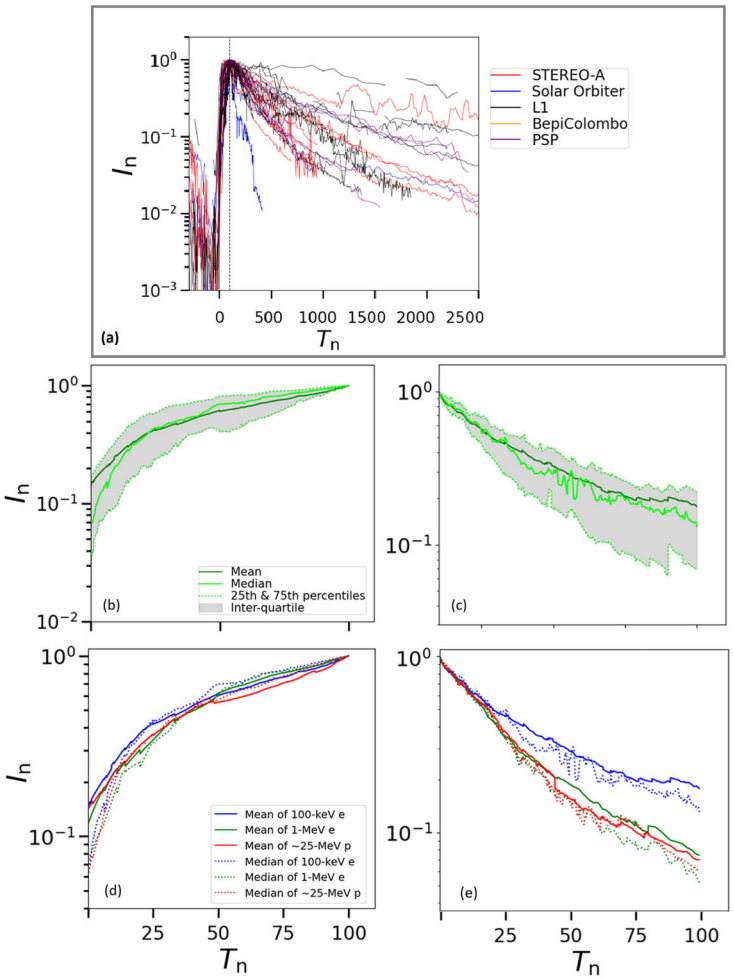

Figure 12. Different steps of SEA applied to SEP profiles of the sample used for this thesis (**Paper III**). The top panel (a) shows the superposed normalized intensity-time profiles, for example, of ∼100 keV electrons for well-connected events. The epoch time selected for the SEA is represented by a black dotted vertical line drawn at Tn = 100. Different colors listed in the legend represent the corresponding observer. The central panel shows the mean (green curve), median (lime solid curve), and the 25th and 75th percentiles (lime dotted curve), with the gray shaded area representing the inter-quartile range for the rise phase (b), and the decay phase (c). The bottom panel shows the final results of the SEA: the mean (solid curve) and the median (dotted curve), for ≥25 MeV protons (red), ∼100 keV (blue) and ∼1 MeV (green) electrons for well-connected events, for the rise (d) and the decay (e) phase. Image credit: Farwa et al. (2026) , reproduced and licensed under CC BY.

superposed and averaged over this time window, considering intervals before, during, and after the epoch time (Chree, 1913). When dealing with a series of events of varying durations, SEA incorporates time normalization to facilitate meaningful comparisons of event characteristics. To achieve this, each event is divided into two intervals: from the event's start to the epoch time, and from the epoch time to a defined end. The length of these intervals is then normalized to a common time axis for all events, effectively stretching or compressing each event profile so that corresponding intervals have equal length across the dataset (Walton and Murphy, 2022). The SEA parameters calculated in general include the mean, median, 25^{th} and 75^{th} percentiles, and inter-quartile range. The mean is calculated as the arithmetic average of all the normalized intensities, and represents the average shape of the superposed SEP profiles of the sample. The median is calculated as the central value representing the central tendency of the sample and is less affected by the outlier trends. The 25^{th} and 75^{th} percentiles are calculated to visualize the overall spread of the sample, representing the level below which 25% and 75% of the data reside, respectively.

Time normalization is applied to the $\sim$100 single-spacecraft profiles, enabling comparison of profile shapes and analysis of the average SEP profile in the SEA (**Paper III**). Normalized intensity-time profiles of the sample superposed together are shown in Fig. 12. For this purpose, the peak time is defined as the epoch time, and the time along the x-axis (Fig. 12, a) is normalized to the rise time of the SEP event as in Eq. (4)

$$T_n = 100\frac{T - T_{\text{onset}}}{T_{\text{peak}} - T_{\text{onset}}} \tag{4}$$

where T_{onset} and T_{peak} are the onset and peak times of an SEP event, respectively, with $T_{\text{peak}} - T_{\text{onset}}$ defined as the "rise time". The value of 100 serves as a scaling factor for normalization and helps to illustrate the evolution from the onset to the peak time in terms of a percentage of the total time span between these two timestamps. We also normalized the intensity along the y-axis (Fig. 12, a) to the peak intensity as $I_{\text{n}} = I/I_{\text{peak}}$ where I is the instantaneous intensity and I_{peak} is the peak intensity of an observed SEP event.

The SEA parameters are calculated for both the rise phase (from the onset to the peak, Fig. 12b,d) and the decay phase (from the peak onward, Fig. 12c,e) for the well-connected and the poorly-connected events as defined by Farwa et al. (2025a).

4.4 Fitting of average SEP profiles

The average intensity-time profiles for both electron energies and protons, obtained from superposed epoch analysis (**Paper III**) are fitted with different empirical models to describe the average behaviour of rise and early decay profiles (Fig. 13). Fitting models are used to quantify important time scales of SEP events, such as rise time,

decay time, and onset delays, and by applying empirical fits to the average SEP profiles, we can compare the characteristics across different particle species, energies, and magnetic connections (Qin and Wang, 2015; Kahler and Ling, 2017; Wang et al., 2022; Musset et al., 2023). This approach not only enhances our understanding of the time evolution of SEP intensity profiles but also aids in predicting rise time and peak intensity, which are crucial for space weather forecasting models (Posner, 2007; Posner and Strauss, 2020; Papaioannou et al., 2022).

In this study (**Paper III**), empirical models with a single fit parameter, such as the exponential law (Fig. 13, blue color) in Eq. (5)

$$I_n = e^{-(T_\mathrm{n}-100)/b} \tag{5}$$

and the power law (Fig. 13, red color) in Eq. (6)

$$I_n = (T_\mathrm{n}/100)^d \tag{6}$$

are applied on the mean SEP profile to describe the average shape of an SEP event.

Wang et al. (2022) fitted the profile of ∼50 MeV energetic proton events with an analytical function of the form in Eq. (7), where a is a scaling factor to monitor the amplitude of peak intensity and t_0 is the onset time. The parameters c and b can be interpreted with respect to radial diffusion in the interplanetary medium following an impulsive injection of particles at the Sun. If the radial diffusion coefficient is given as $D = Ar^B$, then the Wang et al. (2022) model (Eq. (7)) parameters c and b are linked to the diffusion coefficient as $c = 3/(2 - B)$ and $b = (2 - B)^2(D/r^2)$, i.e., c is related to the radial dependence of the diffusion coefficient and $1/b$ is related to the diffusion time scale from the Sun to the observer's location. Wang et al. (2022) concluded that the observer's helio-longitudinal location and the SEP transport conditions are crucial in determining how the intensity profiles of SEPs are shaped.

$$f(t) = a(t - t_0)^{-c} \exp\{-1/[b(t - t_0)]\}. \tag{7}$$

The mean SEP profiles of the sample are also fitted with a similar model in Eq. (8), (Fig. 13, green color), obtained from the diffusion model of Wang et al. (2022) by requiring the profile to start at $T_\mathrm{n} = a$, maximize at $T_\mathrm{n} = 100$, and have a unit value at the maximum,

$$f(T_\mathrm{n}) = \left(\frac{100 - a}{T_n - a}\right)^c \exp\left\{c\left(1 - \frac{100 - a}{T_n - a}\right)\right\}. \tag{8}$$

Kahler and Ling (2017) used a modified Weibull function in Eq. (9)

$$f(t) = (-\alpha/\beta)(t/\beta)^{\alpha-1} \exp\{-(t/\beta)^\alpha\} \tag{9}$$

to fit the $E > 10$ MeV proton profiles. Here, α and β are the fitting parameters and are found to significantly influence on the shape and duration of SEP profile (Kahler and Ling, 2017).

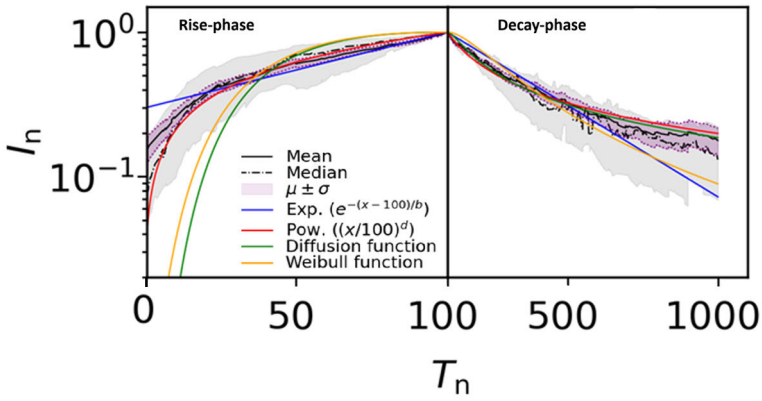

Figure 13. Results of fitting different empirical models to the mean SEP profiles obtained from the SEA of SEP events in the sample used for this thesis, for example, for ∼100 keV electrons in well-connected events. The mean (black solid curve) is fitted with an exponential (blue), power law (red), diffusion function (green), and Weibull function (orange) for the rise (left, zoomed-in x-axis) and the decay (right) phase. The purple and gray shaded areas represent the uncertainty calculated for the mean and the inter-quartile range, respectively. Image credit: Farwa et al. (2026) , reproduced and licensed under CC BY.

The results of the present study are also fitted with a Weibull model, (Fig. 13, orange color) derived from the function of Kahler and Ling (2017) by modifying the profile to start at $T_{\rm n} = m$, obtain its maximum value at $T_{\rm n} = 100$, and have a unit value at the maximum normalized intensity.

$$f(T_{\rm n}) = \left(\frac{T_{\rm n}+m}{100+m}\right)^{l-1} \exp\left[\frac{l-1}{l}\left\{1-\left(\frac{T_{\rm n}+m}{100+m}\right)^{l}\right\}\right] \tag{10}$$

The reduced chi-squares and the fit parameters for each fit are calculated and compared. The fit model with the lowest value of reduced chi-square is taken to be a better fit. The chi-square and the reduced chi-square are the parameters calculated for a fit to test its validity for the model. The chi-square χ^2 measures how well a model fits the data by comparing the data points with the expected points from the model, and is calculated in this study as $\chi^2 = \sum_{i=1}^{N}(R_i/\sigma_i)^2$, where R_i is the residual between the i-th averaged intensity data point and the model value, and σ_i is the standard error of this i-th average value. The reduced chi-square $\chi^2_{\rm red}$, in general, is calculated as $\chi^2_{\rm red} = \chi^2/\nu$, where ν is the number of degrees of freedom ($\nu = N - N_{\rm vars}$, with N as the total number of data points to be fitted and $N_{\rm vars}$ is the number of variables in the fitting model).

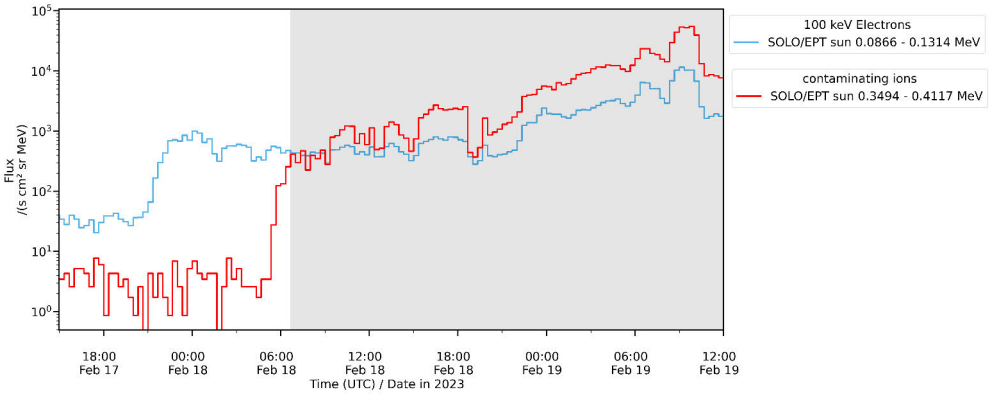

Figure 14. Comparison of ∼100 keV electron (blue) profile with ∼400 keV ions (red) profile to check for ion contamination effects. The contaminated interval is shaded as gray.

4.4.1 Identification of contaminated profile intervals

Some of ∼100 keV electron measurements, obtained with single-detector instruments and affected by energetic ion contamination, are excluded from the data set used for the SEA performed in this study (**Paper III**). The measurements of ∼100 keV electrons from different spacecraft are obtained by instruments based on a single detector layer, which detects the electrons using a foil detection method to stop ions from entering the detector. Incoming ions energetic enough (∼400 keV) to pass the foil, or more energetic ions ($\gg$ 400 keV) that can penetrate the passive collimator of the instrument, may contaminate the electron measurements, mainly when the ion fluxes are higher than the electron fluxes (Wraase et al., 2018; Kartavykh et al., 2025).

For certain SEP event profiles with prolonged decay, it is worth checking for possible ion contamination in electron profiles. The possible ion contamination can be traced by comparing the intensity-time profiles of electrons with those of ions (protons) in the contaminating energy range. The intervals for which the ion profile resembles the electron profile, in both shape and intensity level, are suspected to be contaminated. Identification of ion contamination in ∼100 keV electron measurements is shown in Fig. 14 by comparing the electron profile (Fig. 14, blue) with those of ∼400 keV ions in the contaminating energy range (Fig. 14, red). The contaminated intervals are identified as the gray shaded region where the electron profiles begin to resemble the ion profiles.

5 Summary of the Original Publications

5.1 Paper I: The solar cycle 25 multi-spacecraft solar energetic particle event catalog of the SERPENTINE project

In this paper, we presented a multi-spacecraft SEP event catalog of events observed in the early phase of solar cycle 25, from November 2020 to May 2023, established during the SERPENTINE project. We utilized observations from different instruments on board six different space missions, at five different observer locations (for details, see Sect. 4.1). The catalog reports 45 independent multi-spacecraft SEP events, for $\sim$100 keV electrons, $\sim$1 MeV electrons, and $\geq$25 MeV protons, with a selection criterion for an SEP event based on the observation of energetic protons in the energy range $\sim$25–40 MeV with a significant increase in intensity above the background level, observed by at least two different spacecraft. Observations of 45 independent multi-spacecraft SEP events result in 142 single-spacecraft observations in total. When considering the observations separately for the three energy combinations ($\sim$100 keV electrons, $\sim$1 MeV electrons, and $\geq$25 MeV protons) reported in the catalog, it yields 414 individual events, along with all the key parameters of the SEP events, and associated flares and type II radio bursts (for details, see Sect. 4.1).

With multi-spacecraft measurements treated in a single-spacecraft manner the SERPENTINE SEP event catalog is a valuable database, providing significant statistics of SEP observations to analyze SEP events from the rising phase of solar cycle 25. With the availability of five different viewpoints, located at different heliocentric distances ranging from 0.07 to 1.01 au it provides wide coverage of SEP events, using all possible resources for flare identification (for details, see Sect. 4.1.1). The catalog provides the ratio of peak intensities of relativistic electrons to high-energy ($\geq$25 MeV) protons (for details, see Sect. 4.1.3) which is an important parameter to study the potential contributions of flare and shock towards the source and acceleration processes of SEPs (Cliver and Ling, 2007; Cane et al., 2010; Farwa et al., 2025a).

In comparison to past SEP event catalogs, for example, by Richardson and Cane (2010); Richardson et al. (2014); Vainio et al. (2013); Paassilta et al. (2017), the SERPENTINE SEP event catalog is the most recent and is equipped with modern instruments on board the maximum number of observing viewpoints (five), includ-

ing observations in the inner heliosphere. The observations from the latest space missions, Solar Orbiter and PSP, are included in the catalog. Solar Orbiter/STIX observations enable enhanced identification of flares, including those visible behind the solar limb. The SERPENTINE catalog provides SEP event observations with wider radial and longitudinal coverage. The catalog also provides more precise onset and peak intensity times, by selecting the appropriate time resolution and viewing direction for the earliest onset and highest peak, reducing uncertainties in measurements and making it possible to compare observations from different spacecraft. The SERPENTINE catalog comes with a web interface and related catalogs for shocks and CMEs provided at the SERPENTINE data centre (`https://data.serpentine-h2020.eu`), making it more useful for the community to analyze SEP events and understand their acceleration and transport processes.

The multi-spacecraft observations in the SERPENTINE catalog also help to understand the role of observer location in determining the absolute spread of SEP events. Having information about the spread of an event along with the SEP event and source parameters can help in understanding the contributions of source characteristics and transport effects to the event spread.

An extended version (for details, see Sect. 4.1.4) of the SERPENTINE SEP event catalog has been developed under the SOLER project, and updated the SEP event analysis to December 2023, adding 53 more events to the catalog, resulting in a total of 98 independent SEP events. The onset determination for the extended catalog is based on an even more sensitive method providing the uncertainties in onset time as well (Palmroos et al., 2025).

Author's contribution

The author contributed to the data analysis of the SERPENTINE SEP event catalog, including the flare association from the Solar Orbiter/STIX list (Sect. 4.1.1), the determination of onset and peak intensities for some events (Sect. 4.1.2), and the calculation of the electron-to-proton peak intensity ratio (Sect. 4.1.3). For this purpose, the author re-determined the peak intensities of $\sim$1 MeV electrons for all events using the different methods described in Sect. 4.1.3. The author extended the SERPENTINE SEP event catalog to the SOLER SEP event catalog, updated to December 2023, performing the data analysis for onset and peak determination, calculating the PSP electron count rate to intensity conversion factor, and associating flares and CMEs for all new events (Sect. 4.1.4).

5.2 Paper II: Electron and proton peak intensities as observed by a five-spacecraft fleet in solar cycle 25

The aim of this study was to distinguish between the potential contributions of flare and CME-driven shocks to the acceleration processes of SEPs for electrons and protons and their variation with the energies of SEPs and the magnetic connectivity of the observer to the source. We analyzed high-energy $\geq$25 MeV proton events, described in Sect. 5.1, from the SERPENTINE SEP event catalog (Dresing et al., 2024), including observations from Solar Orbiter, STEREO A, SOHO, Wind, Bepi-Colombo, and PSP. We investigated the correlations between SEP peak intensities, their ratios, onset delays from the flare, and the source parameters for $\sim$100 keV electrons, $\sim$1 MeV electrons, and $\geq$25 MeV protons for both magnetically well-connected and poorly-connected events. The peak intensities of $\sim$100 keV electrons and $\geq$25 MeV protons are taken directly from the SERPENTINE SEP event catalog, while the peak intensities of $\sim$1 MeV electrons used in the analysis are those estimated for the calculation of the electron-to-proton ratio in **Paper I** (Sect. 5.1).

Investigating the correlation between electron and proton peak intensities and their ratio, we observed two distinct populations in the well-connected events, separated at proton peak intensity $I_{\rm p} > 10^{-2}$ (cm^2 sr s MeV)$^{-1}$. The population with higher $I_{\rm p}$ shows a significantly strong correlation between electron and proton peak intensities, suggesting the potential contribution of a single source to the acceleration of electrons and protons. In contrast, the population with lower $I_{\rm p}$ seems to have different acceleration efficiencies for electrons and protons. A single stronger correlation observed between electron and proton peak intensities in poorly-connected events suggests the presence of a single potential source capable of accelerating both electrons and protons.

We concluded that the well-connected events seem to have a blend of flare and shock contributions supporting an earlier analysis by (Cliver and Ling, 2007), with flares accelerating electrons more efficiently. A CME-driven shock can extend beyond well-connected locations, and can connect to poorly-connected sectors, accelerating SEPs with similar efficiency for both electrons and protons. The presence of type II radio bursts was equally observed in our well-connected and poorly-connected events, supporting a major contribution from shocks in both types of events, in contrast to Cliver and Ling (2007), who reported the absence of type II bursts in flare-dominated events.

The strongest correlations are observed between $\sim$100 keV and $\sim$1 MeV electron peak intensities, suggesting that both electron energies always originate from the same source in both well-connected and poorly-connected events. We are unable to distinguish between the potential contributions of flare and shock to the acceleration processes of relativistic and near-relativistic electrons.

Weaker correlations observed between SEP peak intensities and the associated soft X-ray flare intensities, even in the well-connected events, support the dominant contribution coming from shocks only. On the other hand, we do not find any supporting correlations between SEP peak intensities and CME linear speeds. This may be attributed to the fact that SOHO/LASCO CME linear speeds used in the analysis may have uncertainties caused by projection effects. The suggested dominance of shocks is presumably related to the selection criteria of the catalog, which reports only the high-energy $\geq$25 MeV proton events with the constraint that they are observed at two different locations. We also do not notice a preferential presence of slower and narrower CMEs associated with presumably flare-dominated events, as a mixture of all CME speeds (slower and faster) and angular widths (wider and narrower) are reported in six flare-dominated events.

In general, the peak intensities of our sample are anti-correlated with the longitudinal separation angle, with the highest peak intensities observed in well-connected events, as reported earlier (Lario et al., 2006; Lario et al., 2013; Dresing et al., 2014; Richardson et al., 2014). However, significant event-to-event variations showing high peak intensities in poorly-connected events suggest that such poorly-connected events are not dominated by transport effects, but are rather under the direct influence of shocks. The longitudinal distribution of onset delays also shows event-to-event variation. Due to the limited statistics of the sample, we cannot confirm this, but we note a possible asymmetry, based on longer (shorter) electron (proton) onset delays in western (eastern) events.

Author's contribution

The author contributed to developing the analysis approach, conducted the complete data analysis, prepared all figures, and was the primary contributor to writing the manuscript.

5.3 Paper III: Superposed epoch analysis of solar energetic particle events observed in solar cycle 25

In this paper, we investigated the average behaviour of intensity-time profiles of SEP events, with details presented in Sect. 5.1. Superposed epoch analysis was applied to these $\sim$100 profiles for both the well-connected and poorly-connected events, as classified in Sect. 4.2.3. For this purpose, all the SEP profiles were normalized in intensity and time with respect to the peak intensity and rise time, respectively. In order to generalize the average behaviour of an SEP profile, we examined the shapes of the mean and median profiles, and the exponential and power law models applied to the mean normalized profiles, for both the rise and decay phases for all longitudinal sectors.

While comparing the normalized intensity profiles in different longitudinal events, for both electron energies and protons, we observed significant event-to-event variation, ranging from impulsive to gradual decay profiles. The variation in decay profiles may occur due to the time normalization performed with respect to the rise time. However, the mean SEP profile is observed to be quite similar for both electron energies and protons, and does not show any noticeable variation with the magnetic connectivity of the observer to the source.

The fitting results are also compared with a diffusion model (Wang et al., 2022) by applying a modified diffusion function to the mean SEP profiles of the sample. The results are additionally compared with a modified Weibull function model derived from the Weibull model (Kahler and Ling, 2017). Both these models represent the average decay profiles of the sample well, but do not fit the average rise profiles accurately (for details, see Sect. 4.2.3).

The similarity between the electron and proton mean normalized profiles could point to a common acceleration source for both species. Nevertheless, this interpretation remains uncertain, since alternative drivers, such as distinct acceleration regions or transport-related effects, may likewise account for the observed resemblance. The similarity in the mean rise profiles and the onset delay observed between near-relativistic electrons and $\geq$25 MeV protons is an interesting result, supporting the use of the early arrival of relativistic electrons for forecasting high-energy protons, which are the main contributors to radiation hazards. The REleASE forecasting scheme (Posner, 2007), which uses electron observations to predict proton measurements, is supported by our results. Our results, highlighting the similarity between the average rise profiles of relativistic electrons and protons, also support the development of an empirical forecasting model for space weather applications (Papaioannou et al., 2022) to predict proton peak intensity and peak time.

We also investigated the variation in the behaviour of the average SEP profile with heliocentric distance, but we do not observe any difference for different radial locations. Additionally, we do not observe any noticeable difference in the mean SEP profiles of the six events suggested to be flare-dominated by Farwa et al. (2025a) in **Paper II**, in comparison to the rest of the shock-dominated profiles. The discrepancy of superposed epoch analysis in differentiating the potential contributions of flare and shock may be attributed to the limited statistics of the sample.

Author's contribution

The author contributed to developing the analysis approach, conducted the complete data analysis, prepared all figures, and was the primary contributor to writing the manuscript.

6 Conclusion and Outlook

This thesis investigates the relationship between SEP event and source parameters, the characteristics of SEP intensity profiles, and their dependence on the magnetic connection of the observer to the source location, in order to address open questions about SEPs. The focus of this study is to disentangle the relative contribution of the flare and the CME-driven shock in producing large SEP events, to distinguish the acceleration processes for electrons and protons, and to examine how these processes vary with the magnetic connection of the observer. This thesis also explores how to represent an average SEP event for different particle species and energies, and how this average profile behaves with changing magnetic connection.

For this purpose, the author analyzed various parameters of $\sim$1 MeV and $\sim$100 keV electrons and $\geq$25 MeV protons for large SEP events, measured by six different spacecraft at five distinct viewpoints covering a wide longitudinal extent from the source. These measurements are provided in the SERPENTINE SEP event catalog established at the initial stage of this study. By analyzing the ratio of electron to proton peak intensities, six well-connected events were identified as electron-rich and are suggested to be flare-dominated. The correlations found between electron and proton peak intensities indicate that the well-connected events of the sample reflect a combination of flare and shock contributions, with flares being more effective at accelerating electrons, in agreement with similar findings of Cliver and Ling (2007). Based on its broad longitudinal extent, the CME-driven shock is assumed to propagate far beyond well-connected regions. Strong correlations found between electron and proton peak intensities in poorly-connected events suggests that CME-driven shock is the dominant source for accelerating SEPs for poorly-connected observers with similar efficiency for both electrons and protons. Type II radio bursts reported in the SERPENTINE catalog are found to be associated with similar frequency to both well-connected and poorly-connected events, further indicating a dominant shock contribution across all events. The relatively weak correlations between SEP peak intensities and corresponding soft X-ray flare intensities, even for well-connected events, again point to shocks as the dominant acceleration mechanism.

The findings of this study indicate that both electron energy ranges consistently originate from the same source for well-connected and poorly-connected events alike. Overall, the peak intensities of all SEPs show an anti-correlation with the longitudinal separation between the observer and the source location, with the strongest peak

intensities occurring in well-connected events, in agreement with previous studies (Lario et al., 2006; Lario et al., 2013; Dresing et al., 2014; Richardson et al., 2014). However, some exceptions with large peak intensities at poorly connected locations suggest that these events are not governed solely by transport effects. Instead, they may occur when the expanding CME-driven shock extends far enough to maintain magnetic connectivity beyond the nominal 35° boundary.

Overall, the mean normalized SEP profile appears to be similar across both electron energies and protons, with no significant dependence on the observer's magnetic connectivity to the source. The comparable shapes of the average electron and proton profiles could suggest that both particle species likely share a common acceleration origin. The similarity between the average rise profiles and the onset delay of near-relativistic electrons and $\geq$25 MeV protons is particularly noteworthy, as it reinforces the practicality of using the early arrival of relativistic electrons to forecast high-energy protons, the primary drivers of radiation hazards. Our findings therefore support the REleASE forecasting scheme (Posner, 2007), which relies on electron measurements to predict proton intensities. Our results, highlighting the similarity between the average rise profiles of relativistic electrons and protons, also support the development of an empirical forecasting model for space weather applications to predict proton peak intensity and peak time. In this context, a probabilistic model for peak intensities and rise times has been proposed by Papaioannou et al. (2022).

This thesis contributes to the development of the first multi-spacecraft catalog (**Paper I**) of large SEP events for the early phase of Solar Cycle 25, with ongoing extension towards the peak phase. The novelty of the catalog lies in combining observations from the latest heliospheric spacecraft fleet, including PSP, Solar Orbiter, and BepiColombo, together with near-Earth measurements, providing wide longitudinal coverage by unprecedented number of observers (6) at five different viewpoints. Flare identification is further enhanced using behind-the-limb observations from Solar Orbiter/STIX. This dataset improves previous catalogs by extending established event identification methods to a broader multi-spacecraft configuration, while also refining basic SEP onset determination methods.

The thesis provides the first statistical analysis (**Paper II**) of SEP peak-intensities of large SEP events observed by six spacecraft fleet during the early phase of Solar Cycle 25 including a detailed longitudinal classification of SEP events into well- and poorly-connected western and eastern sectors. Building upon established SEP peak-intensity correlation methods, the study supports the earlier findings about the potential contributions from flares and CME-driven shock acceleration.

The application of superposed epoch analysis to SEP events (**Paper III**) produces the first average SEP intensity profile and includes its comparison with four different models. Although the method itself is well established, its application is improved through the newly developed multi-spacecraft dataset.

The study is limited by a relatively small sample confined to early solar cycle 25,

which restricts the robustness of population-based conclusions and the separation of flare and shock contributions. Uncertainties from CME projection effects may cause the ambiguities in correlations with SEPs and flare properties. The selection criterion based on $\geq$25 MeV protons multiple spacecraft detection biases the sample toward large, energetic events, dominated by CME-driven shocks. Additionally, assumptions in magnetic connectivity, radial scaling, and superposed epoch normalization may obscure event-to-event variability and transport effects. The difficulty of the superposed epoch analysis in distinguishing the potential contribution of the flare and the shock may again be linked to the limited size of the event sample.

The results of this study motivate future work utilizing the SOLER catalog (the extended SERPENTINE SEP event catalog) with $\sim$500 single-spacecraft observations, with selection criterion based on single-spacecraft detection, enabling better discrimination of flare- and shock-related SEPs populations and their dependence on the longitudinal and heliocentric location of the observer. The SOLER catalog linking the strong flares and fast CMEs to large SEP events motivates further to investigate the co-existence between CMEs and flares, and their relative role in defining SEP characteristics. Investigating the elemental composition of well- and poorly-connected events of the extended sample, would be useful to disentangle the potential flare and shock contribution. The extended catalog provides some interestingly complicated events as possible case study, to differentiate between the source and transport effects. Improved CME and shock characterization, including 3D kinematics and more accurate magnetic connectivity modeling, is needed to reduce projection and mapping uncertainties. Another important aspect of future studies could be to investigate the role of flare and CME parameters in predicting the occurrence of an SEP event for space weather forecasting. Finally, combining multi-spacecraft observations with physics-based transport and acceleration models will be helpful to disentangle source and transport effects and to further improve SEP forecasting capabilities.

A Use of AI Tools

Artificial Intelligence (AI) tools were used in this thesis solely for language refinement and grammatical corrections. The University of Turku's AI tool, UTU Chat (GPT-4.1), was applied to check and enhance the clarity and grammatical correctness of the text. All suggestions provided by the AI were carefully reviewed and manually implemented by the author. No AI-generated content was used to create original ideas, research findings, or analyses. The intellectual content, analysis, and conclusions of this thesis remain entirely the author's own work. The use of the AI tool was conducted responsibly and in accordance with the academic integrity guidelines of the University of Turku.

List of References

Aguilar-Rodriguez, E., Gopalswamy, N., MacDowall, R., Yashiro, S., and Kaiser, M. L.: A universal characteristic of type II radio bursts, Journal of Geophysical Research: Space Physics, 110, doi:https://doi.org/10.1029/2005JA011171, URL https://agupubs.onlinelibrary.wiley.com/doi/abs/10.1029/2005JA011171, 2005.

Alfvén, H.: Existence of Electromagnetic-Hydrodynamic Waves, Nature, 150, 405–406, doi:10.1038/150405d0, URL https://doi.org/10.1038/150405d0, 1942.

Anastasiadis, A., Lario, D., Papaioannou, A., Kouloumvakos, A., and Vourlidas, A.: Solar energetic particles in the inner heliosphere: status and open questions, Philosophical Transactions of the Royal Society A: Mathematical, Physical and Engineering Sciences, 377, 20180 100, doi:10.1098/rsta.2018.0100, URL https://doi.org/10.1098/rsta.2018.0100, 2019a.

Anastasiadis, A., Lario, D., Papaioannou, A., Kouloumvakos, A., and Vourlidas, A.: Solar energetic particles in the inner heliosphere: status and open questions, Philosophical Transactions of the Royal Society A: Mathematical, Physical and Engineering Sciences, 377, 20180 100, doi:10.1098/rsta.2018.0100, URL https://royalsocietypublishing.org/doi/abs/10.1098/rsta.2018.0100, 2019b.

Axford, W. I., Leer, E., and Skadron, G.: The Acceleration of Cosmic Rays by Shock Waves, in: International Cosmic Ray Conference, vol. 11 of *International Cosmic Ray Conference*, p. 132, 1977.

Bai, T. and Sturrock, P. A.: Classification of solar flares, Ann. Rev. Astron. Astrophys., 27, 421–467, doi:10.1146/annurev.aa.27.090189.002225, 1989.

Baker, D. N., Li, X., Pulkkinen, A., Ngwira, C. M., Mays, M. L., Galvin, A. B., and Simunac, K. D. C.: A major solar eruptive event in July 2012: Defining extreme space weather scenarios, Space Weather, 11, 585–591, doi:https://doi.org/10.1002/swe.20097, URL https://agupubs.onlinelibrary.wiley.com/doi/abs/10.1002/swe.20097, 2013.

Beck, P., Latocha, M., Rollet, S., and Stehno, G.: TEPC reference measurements at aircraft altitudes during a solar storm, Advances in Space Research, 36, 1627–1633, doi:https://doi.org/10.1016/j.asr.2005.05.035, URL https://www.sciencedirect.com/science/article/pii/S0273117705005946, space Life Sciences: Aircraft and Space Radiation Environment, 2005.

Bell, A. R.: The acceleration of cosmic rays in shock fronts - I., Mon. Not. R. Astron. Soc., 182, 147–156, doi:10.1093/mnras/182.2.147, 1978.

Benkhoff, J., Murakami, G., Baumjohann, W., Besse, S., Bunce, E., Casale, M., Cremosese, G., Glassmeier, K. H., Hayakawa, H., Heyner, D., Hiesinger, H., Huovelin, J., Hussmann, H., Iafolla, V., Iess, L., Kasaba, Y., Kobayashi, M., Milillo, A., Mitrofanov, I. G., Montagnon, E., Novara, M., Orsini, S., Quemerais, E., Reininghaus, U., Saito, Y., Santoli, F., Stramaccioni, D., Sutherland, O., Thomas, N., Yoshikawa, I., and Zender, J.: BepiColombo - Mission Overview and Science Goals, Space Sci. Rev., 217, 90, doi:10.1007/s11214-021-00861-4, 2021.

Benz, A. O. and Thejappa, G.: Radio emission of coronal shock waves, Astron. Astrophys., 202, 267–274, 1988.

Blandford, R. D. and Ostriker, J. P.: Particle acceleration by astrophysical shocks., Astrophys. J. Lett., 221, L29–L32, doi:10.1086/182658, 1978.

Bochsler, P.: Composition of matter in the heliosphere, Proceedings of the International Astronomical Union, 4, 17–28, doi:10.1017/S1743921309029044, 2008.

Brüdern, M., Dresing, N., Heber, B., Wimmer-Schweingruber, R., Klassen, A., Berger, L., and Kühl, P.: Determination of SEP Anisotropies Based on Four-Sector Measurements, Central European Astrophysical Bulletin, 42, 2, 2018.

Bucik, R., Dayeh, M. A., Starkey, M., and Desai, M.: Properties of the suprathermal ion population in fast and slow solar wind structures as measured by the Parker Solar Probe, in: 44th COSPAR Scientific Assembly. Held 16-24 July, vol. 44, p. 1476, 2022.

Cane, H. V.: The evolution of interplanetary shocks, Journal of Geophysical Research: Space Physics, 90, 191–197, doi:https://doi.org/10.1029/JA090iA01p00191, URL https://agupubs.onlinelibrary.wiley.com/doi/abs/10.1029/JA090iA01p00191, 1985.

Cane, H. V.: Longitudinal extents of coronal/interplanetary shocks, in: AIP Conference Proceedings, vol. 374, pp. 124–130, AIP, doi:10.1063/1.50948, URL http://adsabs.harvard.edu/abs/1996AIPC..374..124C, 1996.

Cane, H. V. and Reames, D. V.: The relationship between energetic particles and flare properties for impulsive solar flares, Astrophys. J.Supplement Series, 73, 253–258, URL http://adsabs.harvard.edu/abs/1990ApJS...73..253C, 1990.

Cane, H. V., Reames, D. V., and von Rosenvinge, T. T.: The role of interplanetary shocks in the longitude distribution of solar energetic particles, J. Geophys. Res., 93, 9555–9567, doi:10.1029/JA093iA09p09555, 1988.

Cane, H. V., von Rosenvinge, T. T., Cohen, C. M. S., and Mewaldt, R. A.: Two components in major solar particle events, Geophys. Res. Lett., 30, 8017, doi:10.1029/2002GL016580, 2003.

Cane, H. V., Mewaldt, R. A., Cohen, C. M. S., and von Rosenvinge, T. T.: Role of flares and shocks in determining solar energetic particle abundances, Journal of Geophysical Research (Space Physics), 111, A06S90, doi:10.1029/2005JA011071, 2006.

Cane, H. V., Richardson, I. G., and von Rosenvinge, T. T.: A study of solar energetic particle events of 1997-2006: Their composition and associations, Journal of Geophysical Research (Space Physics), 115, A08101, doi:10.1029/2009JA014848, 2010.

Chang, Q., Xu, X., Wang, X., Ye, Y., Xu, Q., Wang, J., Wang, M., Zhou, Z., Luo, L., Cheng, S., and He, P.: The Solar Wind Parker Spiral Angle Distributions and Variations at 1 au, The Astrophysical Journal, 931, 105, doi:10.3847/1538-4357/ac6bf3, URL https://dx.doi.org/10.3847/1538-4357/ac6bf3, 2022.

Chree, C.: III. Some phenomena of sunspots and of terrestrial magnetism at Kew Observatory, Philosophical Transactions of the Royal Society of London. Series A, Containing Papers of a Mathematical or Physical Character, 212, 75–116, doi:10.1098/rsta.1913.0003, URL https://royalsocietypublishing.org/doi/abs/10.1098/rsta.1913.0003, 1913.

Cliver, E.: The 1859 space weather event: Then and now, Advances in Space Research, 38, 119–129, doi:https://doi.org/10.1016/j.asr.2005.07.077, URL https://www.sciencedirect.com/science/article/pii/S0273117705010215, the Great Historical Geomagnetic Storm of 1859: A Modern Look, 2006.

Cliver, E. W. and Dietrich, W. F.: The 1859 space weather event revisited: limits of extreme activity, Journal of Space Weather and Space Climate, 3, A31, doi:10.1051/swsc/2013053, 2013.

Cliver, E. W. and Ling, A. G.: Electrons and Protons in Solar Energetic Particle Events, Astrophys. J., 658, 1349–1356, doi:10.1086/511737, 2007.

Cliver, E. W., Kahler, S. W., Neidig, D. F., Cane, H. V., Richardson, I. G., Kallenrode, M.-B., and Wibberenz, G.: Extreme "Propagation" of Solar Energetic Particles, p. 257, URL http://adsabs.harvard.edu/abs/1995ICRC....4..257C, 1995.

Cliver, E. W., Kahler, S. W., and Reames, D. V.: Coronal Shocks and Solar Energetic Proton Events, The Astrophysical Journal, 605, 902, doi:10.1086/382651, URL https://dx.doi.org/10.1086/382651, 2004.

Cucinotta, F., Badhwar, G., Saganti, P., Schimmerling, W., Wilson, J., Peterson, L., and Dicello, J.: Space Radiation Cancer Risk Projections for Exploration Missions: Uncertainty Reduction and Mitigation, doi:10.13140/RG.2.2.27982.05445, 2002.

Dayeh, M.: Coronal mass ejections# 4, in: Handbook of Cosmic Hazards and Planetary Defense, pp. 81–98, 2015.

Dayeh, M. A., Desai, M. I., Dwyer, J. R., Rassoul, H. K., Mason, G. M., and Mazur, J. E.: COMPOSITION AND SPECTRAL PROPERTIES OF THE 1 AU QUIET-TIME SUPRATHERMAL ION POPULATION DURING SOLAR CYCLE 23, The Astrophysical Journal, 693, 1588, doi:10.1088/0004-637X/693/2/1588, URL https://doi.org/10.1088/0004-637X/693/2/1588, 2009.

Dayeh, M. A., Desai, M. I., Kozarev, K., Schwadron, N. A., Townsend, L. W., PourArsalan, M., Zeitlin, C., and Hatcher, R. B.: Modeling proton intensity gradients and radiation dose equivalents in the inner heliosphere using EMMREM: May 2003 solar events, Space Weather, 8, doi:https://doi.org/10.1029/2009SW000566, URL https://agupubs.onlinelibrary.wiley.com/doi/abs/10.1029/2009SW000566, 2010.

Desai, M. and Giacalone, J.: Large gradual solar energetic particle events, Living Reviews in Solar Physics, 13, 3, doi:10.1007/s41116-016-0002-5, 2016.

Desai, M. I., Mason, G. M., Dwyer, J. R., Mazur, J. E., Gold, R. E., Krimigis, S. M., Smith, C. W., and Skoug, R. M.: Evidence for a Suprathermal Seed Population of Heavy Ions Accelerated by Interplanetary Shocks near 1 AU, Astrophys. J., 588, 1149–1162, doi:10.1086/374310, 2003.

Desai, M. I., Dayeh, M. A., and Mason, G. M.: Origin of Quiet-Time Suprathermal Tails Near 1 AU, AIP Conference Proceedings, 1216, 635–638, doi:10.1063/1.3395946, URL https://doi.org/10.1063/1.3395946, 2010.

Domingo, V., Fleck, B., and Poland, A. I.: The SOHO Mission: an Overview, Sol. Phys., 162, 1–37, doi:10.1007/BF00733425, 1995.

Dresing, N., Gómez-Herrero, R., Klassen, A., Heber, B., Kartavykh, Y., and Dröge, W.: The Large Longitudinal Spread of Solar Energetic Particles During the 17 January 2010 Solar Event, Sol. Phys., 281, 281–300, doi:10.1007/s11207-012-0049-y, 2012.

Dresing, N., Gómez-Herrero, R., Heber, B., Klassen, A., Malandraki, O., Dröge, W., and Kartavykh, Y.: Statistical survey of widely spread out solar electron events observed with STEREO and ACE with special attention to anisotropies, Astron. Astrophys., 567, A27, doi:10.1051/0004-6361/201423789, 2014.

Dresing, N., Theesen, S., Klassen, A., and Heber, B.: Efficiency of particle acceleration at interplanetary shocks: Statistical study of STEREO observations, Astron. Astrophys., 588, A17, doi:10.1051/0004-6361/201527853, 2016.

Dresing, N., Effenberger, F., Gómez-Herrero, R., Heber, B., Klassen, A., Kollhoff, A., Richardson, I., and Theesen, S.: Statistical Results for Solar Energetic Electron Spectra Observed over 12 yr with STEREO/SEPT, Astrophys. J., 889, 143, doi:10.3847/1538-4357/ab64e5, 2020.

Dresing, N., Kouloumvakos, A., Vainio, R., and Rouillard, A.: On the Role of Coronal Shocks for Accelerating Solar Energetic Electrons, Astrophys. J. Lett., 925, L21, doi:10.3847/2041-8213/ac4ca7, 2022.

Dresing, N., Rodríguez-García, L., Jebaraj, I. C., Warmuth, A., Wallace, S., Balmaceda, L., Podladchikova, T., Strauss, R. D., Kouloumvakos, A., Palmroos, C., Krupar, V., Gieseler, J., Xu, Z., Mitchell, J. G., Cohen, C. M. S., de Nolfo, G. A., Palmerio, E., Carcaboso, F., Kilpua, E. K. J., Trotta, D., Auster, U., Asvestari, E., da Silva, D., Dröge, W., Getachew, T., Gómez-Herrero, R., Grande, M., Heyner, D., Holmström, M., Huovelin, J., Kartavykh, Y., Laurenza, M., Lee, C. O., Mason, G., Maksimovic, M., Mieth, J., Murakami, G., Oleynik, P., Pinto, M., Pulupa, M., Richter, I., Rodríguez-Pacheco, J., Sánchez-Cano, B., Schuller, F., Ueno, H., Vainio, R., Vecchio, A., Veronig, A. M., and Wijsen, N.: The 17 April 2021 widespread solar energetic particle event, Astron. Astrophys., p. accepted, doi:10.1051/0004-6361/202345938, 2023.

Dresing, N., Yli-Laurila, A., Valkila, S., Gieseler, J., Morosan, D. E., Farwa, G. U., Kartavykh, Y., Palmroos, C., Jebaraj, I., Jensen, S., Kühl, P., Heber, B., Espinosa, F., Gómez-Herrero, R., Kilpua,

E., Linho, V. V., Oleynik, P., Hayes, L. A., Warmuth, A., Schuller, F., Collier, H., Xiao, H., Asvestari, E., Trotta, D., Mitchell, J. G., Cohen, C. M. S., Labrador, A. W., Hill, M. E., and Vainio, R.: The solar cycle 25 multi-spacecraft solar energetic particle event catalog of the SERPENTINE project, Astron. Astrophys., 687, A72, doi:10.1051/0004-6361/202449831, 2024.

Dresing, N., Jebaraj, I. C., Wijsen, N., Palmerio, E., Rodríguez-García, L., Palmroos, C., Gieseler, J., Jarry, M., Asvestari, E., Mitchell, J. G., Cohen, C. M. S., Lee, C. O., Wei, W., Ramstad, R., Riihonen, E., Oleynik, P., Kouloumvakos, A., Warmuth, A., Sánchez-Cano, B., Ehresmann, B., Dunn, P., Dudnik, O., and Mac Cormack, C.: The reason for the widespread energetic storm particle event of 13 March 2023, Astron. Astrophys., 695, A127, doi:10.1051/0004-6361/202453596, 2025.

Dröge, W.: Solar Particle Transport in a Dynamical Quasi-linear Theory, Astrophys. J., 589, 1027–1039, doi:10.1086/374812, 2003.

Dröge, W., Kartavykh, Y. Y., Dresing, N., and Klassen, A.: Multi-spacecraft Observations and Transport Modeling of Energetic Electrons for a Series of Solar Particle Events in August 2010, Astrophys. J., 826, 134, doi:10.3847/0004-637X/826/2/134, 2016.

Farwa, G. U., Dresing, N., Gieseler, J., Vuorinen, L., Richardson, I. G., Palmroos, C., Valkila, S., Heber, B., Jensen, S., Kühl, P., Rodríguez-García, L., and Vainio, R.: Electron and proton peak intensities as observed by a five-spacecraft fleet in solar cycle 25, Astron. Astrophys., 693, A198, doi:10.1051/0004-6361/202450945, URL https://doi.org/10.1051/0004-6361/202450945, 2025a.

Farwa, G. U., Dresing, N., Gieseler, J., Vuorinen, L., Richardson, I. G., Palmroos, C., Valkila, S., Heber, B., Jensen, S., Kühl, P., Rodríguez-García, L., and Vainio, R.: Electron and proton peak intensities as observed by a five-spacecraft fleet in solar cycle 25 (Corrigendum), Astron. Astrophys., 699, C2, doi:10.1051/0004-6361/202555825e, 2025b.

Farwa, G. U., Dresing, N., Vuorinen, L., Palmroos, C., Gieseler, J., and Vainio, R.: Superposed epoch analysis of solar energetic particle events observed in solar cycle 25, Advances in Space Research, 77, 1304–1320, doi:https://doi.org/10.1016/j.asr.2025.10.099, URL https://www.sciencedirect.com/science/article/pii/S0273117725012694, 2026.

Fiori, R. A. D., Kumar, V. V., Boteler, D. H., and Terkildsen, M. B.: Occurrence rate and duration of space weather impacts on high-frequency radio communication used by aviation, J. Space Weather Space Clim., 12, 21, doi:10.1051/swsc/2022017, URL https://doi.org/10.1051/swsc/2022017, 2022.

Forbush, S. E.: Three Unusual Cosmic-Ray Increases Possibly Due to Charged Particles from the Sun, Phys. Rev., 70, 771–772, doi:10.1103/PhysRev.70.771, URL https://link.aps.org/doi/10.1103/PhysRev.70.771, 1946.

Fox, N. J., Velli, M. C., Bale, S. D., Decker, R., Driesman, A., Howard, R. A., Kasper, J. C., Kinnison, J., Kusterer, M., Lario, D., Lockwood, M. K., McComas, D. J., Raouafi, N. E., and Szabo, A.: The Solar Probe Plus Mission: Humanity's First Visit to Our Star, Space Sci. Rev., 204, 7–48, doi:10.1007/s11214-015-0211-6, 2016.

Ganse, U., Kilian, P., Vainio, R., and Spanier, F.: Emission of Type II Radio Bursts - Single-Beam versus Two-Beam Scenario, Solar Physics, 280, doi:10.1007/s11207-012-0077-7, 2012.

Gergely, T. E. and Erickson, W. C.: Decameter Storm Radiation, I, Sol. Phys., 42, 467–486, doi:10.1007/BF00149927, 1975.

Getley, I. L., Duldig, M. L., Smart, D. F., and Shea, M. A.: Radiation dose along North American transcontinental flight paths during quiescent and disturbed geomagnetic conditions, Space Weather, 3, doi:https://doi.org/10.1029/2004SW000110, URL https://agupubs.onlinelibrary.wiley.com/doi/abs/10.1029/2004SW000110, 2005.

Gieseler, J., Dresing, N., Palmroos, C., Freiherr von Forstner, J. L., Price, D. J., Vainio, R., Kouloumvakos, A., Rodríguez-García, L., Trotta, D., Génot, V., Masson, A., Roth, M., and Veronig, A.: Solar-MACH: An open-source tool to analyze solar magnetic connection configurations, Frontiers in Astronomy and Space Sciences, 9, 384, doi:10.3389/fspas.2022.1058810, 2023.

Gopalswamy, N., Yashiro, S., Michalek, G., Xie, H., Mäkelä, P., Vourlidas, A., and Howard, R. A.: A Catalog of Halo Coronal Mass Ejections from SOHO, Sun and Geosphere, 5, 7–16, 2010.

Gosling, J. T.: Coronal mass ejections and magnetic flux ropes in interplanetary space, Geophysical Monograph Series, 58, 343–364, doi:10.1029/GM058p0343, 1990.

Gosling, J. T.: The solar flare myth, J. Geophys. Res., 98, 18 937–18 950, doi:10.1029/93JA01896, 1993.

Gosling, J. T. and Pizzo, V. J.: Formation and Evolution of Corotating Interaction Regions and their Three Dimensional Structure, Space Science Reviews, 89, 21–52, doi:10.1023/A:1005291711900, URL https://doi.org/10.1023/A:1005291711900, 1999.

Grappin, R., Mangeney, A., and Marsch, E.: On the origin of solar wind MHD turbulence: Helios data revisited, J. Geophys. Res., 95, 8197–8209, doi:10.1029/JA095iA06p08197, 1990.

Haggerty, D. K. and Roelof, E. C.: Impulsive Near-relativistic Solar Electron Events: Delayed Injection with Respect to Solar Electromagnetic Emission, The Astrophysical Journal, 579, 841, doi:10.1086/342870, URL https://dx.doi.org/10.1086/342870, 2002.

Hernandez Camero, J., Green, L. M., and Piñel Neparidze, A.: Identifying Coronal Mass Ejection Active Region Sources: An Automated Approach, Astrophys. J., 979, 63, doi:10.3847/1538-4357/ad9b27, 2025.

Horne, R. B., Glauert, S. A., Meredith, N. P., Boscher, D., Maget, V., Heynderickx, D., and Pitchford, D.: Space weather impacts on satellites and forecasting the Earth's electron radiation belts with SPACECAST, Space Weather, 11, 169–186, doi:https://doi.org/10.1002/swe.20023, URL https://agupubs.onlinelibrary.wiley.com/doi/abs/10.1002/swe.20023, 2013.

Huovelin, J., Vainio, R., Kilpua, E., Lehtolainen, A., Korpela, S., Esko, E., Muinonen, K., Bunce, E., Martindale, A., Grande, M., Andersson, H., Nenonen, S., Lehti, J., Schmidt, W., Genzer, M., Vihavainen, T., Saari, J., Peltonen, J., Valtonen, E., Talvioja, M., Portin, P., Narendranath, S., Jarvinen, R., Okada, T., Milillo, A., Laurenza, M., Heino, E., and Oleynik, P.: Solar Intensity X-Ray and Particle Spectrometer SIXS: Instrument Design and First Results, Space Science Reviews, 216, doi:10.1007/s11214-020-00717-3, 2020.

Hutton, J. and Morgan, H.: Automated detection of coronal mass ejections in three-dimensions using multi-viewpoint observations, Astron. Astrophys., 599, A68, doi:10.1051/0004-6361/201629516, 2017.

Huttunen-Heikinmaa, K., Valtonen, E., and Laitinen, T.: Proton and helium release times in SEP events observed with SOHO/ERNE, Astron. Astrophys., 442, 673–685, doi:10.1051/0004-6361:20042620, 2005.

Hyndman, R. A., Dalla, S., Laitinen, T., Hutchinson, A., Cohen, C. M. S., and Wimmer-Schweingruber, R. F.: Multi-spacecraft observations of the decay phase of solar energetic particle events, Astron. Astrophys., 694, A242, doi:10.1051/0004-6361/202453012, 2025.

Iucci, N., Levitin, A. E., Belov, A. V., Eroshenko, E. A., Ptitsyna, N. G., Villoresi, G., Chizhenkov, G. V., Dorman, L. I., Gromova, L. I., Parisi, M., Tyasto, M. I., and Yanke, V. G.: Space weather conditions and spacecraft anomalies in different orbits, Space Weather, 3, doi:https://doi.org/10.1029/2003SW000056, URL https://agupubs.onlinelibrary.wiley.com/doi/abs/10.1029/2003SW000056, 2005.

Kahler, S.: The morphological and statistical properties of solar X-ray events with long decay times., Astrophys. J., 214, 891–897, doi:10.1086/155319, 1977.

Kahler, S., Cliver, E., and Ling, A.: Validating the proton prediction system (PPS), Journal of Atmospheric and Solar-Terrestrial Physics, 69, 43–49, doi:https://doi.org/10.1016/j.jastp.2006.06.009, URL https://www.sciencedirect.com/science/article/pii/S1364682606002306, challenges to Modeling the Sun-Earth System, a Workshop, 2007.

Kahler, S. W.: The role of the big flare syndrome in correlations of solar energetic proton fluxes and associated microwave burst parameters, J. Geophys. Res., 87, 3439–3448, doi:10.1029/JA087iA05p03439, 1982.

Kahler, S. W.: Solar flares and coronal mass ejections, Annual Review of Astron. Astrophys., 30, 113–141, URL http://adsabs.harvard.edu/abs/1992ARA%26A..30..113K, 1992.

Kahler, S. W.: The correlation between solar energetic particle peak intensities and speeds of coronal mass ejections: Effects of ambient particle intensities and energy spectra, Journal of Geophysical Research: Space Physics, 106, 20 947–20 955, doi:https://doi.org/10.1029/2000JA002231, URL https://agupubs.onlinelibrary.wiley.com/doi/abs/10.1029/2000JA002231, 2001.

Kahler, S. W. and Ling, A. G.: Characterizing Solar Energetic Particle Event Profiles with Two-Parameter Fits, Solar Physics, 292, 59, doi:10.1007/s11207-017-1085-4, URL https://doi.org/10.1007/s11207-017-1085-4, 2017.

Kaiser, M. L., Kucera, T. A., Davila, J. M., St. Cyr, O. C., Guhathakurta, M., and Christian, E.: The STEREO Mission: An Introduction, Space Sci. Rev., 136, 5–16, doi:10.1007/s11214-007-9277-0, 2008.

Kartavykh, Y., Rodríguez-García, L., Heber, B., Wimmer-Schweingruber, R. F., Trotta, D., Gieseler, J., Dröge, H., Kollhoff, A., Dröge, W., Kilpua, E., Horbury, T., Espinosa Lara, F., Gómez-Herrero, R., Rodríguez-Pacheco, J., Lario, D., Dresing, N., Klassen, A., and Vainio, R.: A statistical study of energetic particle events associated with interplanetary shocks observed by Solar Orbiter in solar cycle 25, Astron. Astrophys., 699, A24, doi:10.1051/0004-6361/202553775, 2025.

Kecskemety, K., Daibog, E., Logachev, Y., and Kota, J.: The decay phase of solar energetic particle events, Journal of Geophysical Research, 114, doi:10.1029/2008JA013730, 2009.

Kellermann, K. I., Bouton, E. N., and Brandt, S. S.: The Postwar Explosion in Radio Astronomy: The US Falls Behind, pp. 35–75, Springer International Publishing, Cham, doi:10.1007/978-3-030-32345-5_2, URL https://doi.org/10.1007/978-3-030-32345-5_2, 2020.

Kilpua, E., Good, S., Dresing, N., Vainio, R., Davies, E., Forsyth, R., Gieseler, J., Lavraud, B., Asvestari, E., Morosan, D., Pomoell, J., Price, D., Heyner, D., Horbury, T., Angelini, V., O'Brien, H., Evans, V., Rodriguez-Pacheco, J., Gómez-Herrero, R., Ho, G., and Wimmer-Schweingruber, R.: Multi-spacecraft observations of the sheath structure of an interplanetary coronal mass ejection and related energetic ion enhancement, Astron. Astrophys., doi:10.1051/0004-6361/202140838, 2021.

Klecker, B.: Current understanding of SEP acceleration and propagation, Journal of Physics: Conference Series, 409, 012 015, doi:10.1088/1742-6596/409/1/012015, URL https://dx.doi.org/10.1088/1742-6596/409/1/012015, 2013.

Klein, K.-L. and Dalla, S.: Acceleration and Propagation of Solar Energetic Particles, Space Sci. Rev., 212, 1107–1136, doi:10.1007/s11214-017-0382-4, 2017.

Klimchuk, J. A.: Theory of Coronal Mass Ejections, pp. 143–157, American Geophysical Union (AGU), doi:https://doi.org/10.1029/GM125p0143, URL https://agupubs.onlinelibrary.wiley.com/doi/abs/10.1029/GM125p0143, 2001.

Kollhoff, A., Berger, L., Brüdern, M., Dresing, N., Eldrum, S., Fleth, S., Gómez-Herrero, R., Heber, B., Kühl, P., Pacheco, D., Rodríguez-García, L., Rodríguez-Pacheco, J., Wimmer-Schweingruber, R. F., and Xu, Z.: Multi-spacecraft observations of near-relativistic electron events at different radial distances, Astron. Astrophys., 675, A155, doi:10.1051/0004-6361/202345955, 2023.

Kouloumvakos, A., Nindos, A., Valtonen, E., Alissandrakis, C. E., Malandraki, O., Tsitsipis, P., Kontogeorgos, A., Moussas, X., and Hillaris, A.: Properties of solar energetic particle events inferred from their associated radio emission, Astron. Astrophys., 580, A80, doi:10.1051/0004-6361/201424397, 2015.

Kouloumvakos, A., Rouillard, A. P., Wu, Y., Vainio, R., Vourlidas, A., Plotnikov, I., Afanasiev, A., and Önel, H.: Connecting the Properties of Coronal Shock Waves with Those of Solar Energetic Particles, Astrophys. J., 876, 80, doi:10.3847/1538-4357/ab15d7, 2019.

Krucker, S., Kontar, E. P., Christe, S., and Lin, R. P.: Solar Flare Electron Spectra at the Sun and near the Earth, Astrophys. J., 663, L109–L112, doi:10.1086/519373, URL http://adsabs.harvard.edu/abs/2007ApJ...663L.109K, 2007.

Krymskii, G. F.: A regular mechanism for the acceleration of charged particles on the front of a shock wave, Akademiia Nauk SSSR Doklady, 234, 1306–1308, 1977.

Kumari, A., Morosan, D. E., Kilpua, E. K. J., and Daei, F.: Type II radio bursts and their association with coronal mass ejections in solar cycles 23 and 24, Astron. Astrophys., 675, A102, doi:10.1051/0004-6361/202244015, 2023.

Lario, D.: Advances in modeling gradual solar energetic particle events, Advances in Space Research, 36, 2279–2288, URL https://api.semanticscholar.org/CorpusID:19907434, 2005.

Lario, D. and Decker, R. B.: The energetic storm particle event of October 20, 1989, Geophys. Res. Lett., 29, 1393, doi:10.1029/2001GL014017, 2002.

Lario, D. and Karelitz, A.: Influence of interplanetary coronal mass ejections on the peak intensity of solar energetic particle events, Journal of Geophysical Research: Space Physics, 119, 4185–4209, doi:https://doi.org/10.1002/2014JA019771, URL https://agupubs.onlinelibrary.wiley.com/doi/abs/10.1002/2014JA019771, 2014.

Lario, D., Kallenrode, M.-B., Decker, R. B., Roelof, E. C., Krimigis, S. M., Aran, A., and Sanahuja, B.: Radial and Longitudinal Dependence of Solar 4-13 MeV and 27-37 MeV Proton Peak Intensities and Fluences: Helios and IMP 8 Observations, Astrophys. J., 653, 1531–1544, doi:10.1086/508982, 2006.

Lario, D., Aran, A., Gómez-Herrero, R., Dresing, N., Heber, B., Ho, G. C., Decker, R. B., and Roelof, E. C.: Longitudinal and Radial Dependence of Solar Energetic Particle Peak Intensities: STEREO, ACE, SOHO, GOES, and MESSENGER Observations, Astrophys. J., 767, 41, doi:10.1088/0004-637X/767/1/41, 2013.

Lario, D., Kwon, R.-Y., Vourlidas, A., Raouafi, N. E., Haggerty, D. K., Ho, G. C., Anderson, B. J., Papaioannou, A., Gómez-Herrero, R., Dresing, N., and Riley, P.: Longitudinal Properties of a Widespread Solar Energetic Particle Event on 2014 February 25: Evolution of the Associated CME Shock, Astrophys. J., 819, 72, doi:10.3847/0004-637X/819/1/72, 2016.

Lario, D., Kwon, R.-Y., Richardson, I. G., Raouafi, N. E., Thompson, B. J., von Rosenvinge, T. T., Mays, M. L., Mäkelä, P. A., Xie, H., Bain, H. M., Zhang, M., Zhao, L., Cane, H. V., Papaioannou, A., Thakur, N., and Riley, P.: The Solar Energetic Particle Event of 2010 August 14: Connectivity with the Solar Source Inferred from Multiple Spacecraft Observations and Modeling, Astrophys. J., 838, 51, doi:10.3847/1538-4357/aa63e4, 2017.

Lario, D., Wijsen, N., Kwon, R. Y., Sánchez-Cano, B., Richardson, I. G., Pacheco, D., Palmerio, E., Stevens, M. L., Szabo, A., Heyner, D., Dresing, N., Gómez-Herrero, R., Carcaboso, F., Aran, A., Afanasiev, A., Vainio, R., Riihonen, E., Poedts, S., Brüden, M., Xu, Z. G., and Kollhoff, A.: Influence of Large-scale Interplanetary Structures on the Propagation of Solar Energetic Particles: The Multispacecraft Event on 2021 October 9, Astrophys. J., 934, 55, doi:10.3847/1538-4357/ac6efd, 2022.

Li, T. M., Li, C., Chen, P. F., and Ding, W. J.: Particle-in-cell simulation of plasma emission in solar radio bursts, Astron. Astrophys., 653, A169, doi:10.1051/0004-6361/202140973, 2021.

Lin, R. P.: Energetic solar electrons in the interplanetary medium, Sol. Phys., 100, 537–561, doi:10.1007/BF00158444, 1985.

Lin, R. P., Anderson, K. A., Ashford, S., Carlson, C., Curtis, D., Ergun, R., Larson, D., McFadden, J., McCarthy, M., Parks, G. K., Rème, H., Bosqued, J. M., Coutelier, J., Cotin, F., D'Uston, C., Wenzel, K.-P., Sanderson, T. R., Henrion, J., Ronnet, J. C., and Paschmann, G.: A Three-Dimensional Plasma and Energetic Particle Investigation for the Wind Spacecraft, Space Sci. Rev., 71, 125–153, doi:10.1007/BF00751328, 1995.

Lucas, J. M.: Counted Data CUSUM's, Technometrics, 27, 129–144, URL http://www.jstor.org/stable/1268761, 1985.

Lugaz, N., Temmer, M., Wang, Y., and Farrugia, C. J.: The Interaction of Successive Coronal Mass Ejections: A Review, Sol. Phys., 292, 64, doi:10.1007/s11207-017-1091-6, 2017.

Lysenko, A., Frederiks, D., Fleishman, G., Aptekar, R., Altyntsev, A., Golenetskii, S., Svinkin, D., Ulanov, M., Tsvetkova, A., and Ridnaia, A.: X-ray and gamma-ray emission of solar flares, Uspekhi Fizicheskih Nauk, 190, doi:10.3367/UFNr.2019.06.038757, 2019.

Masías-Meza, J. J., Dasso, S., Démoulin, P., Rodriguez, L., and Janvier, M.: Superposed epoch study of ICME sub-structures near Earth and their effects on Galactic cosmic rays, Astron. Astrophys., 592, A118, doi:10.1051/0004-6361/201628571, 2016.

Mason, G. M., Gloeckler, G., and Hovestadt, D.: Temporal variations of nucleonic abundances in solar flare energetic particle events. II - Evidence for large-scale shock acceleration, Astrophys. J., 280, 902–916, doi:10.1086/162066, 1984.

Masson, S., Démoulin, P., Dasso, S., and Klein, K.-L.: The interplanetary magnetic structure that guides solar relativistic particles, Astron. Astrophys., 538, A32, doi:10.1051/0004-6361/201118145, URL https://doi.org/10.1051/0004-6361/201118145, 2012.

McComas, D. J., Alexander, N., Angold, N., Bale, S., Beebe, C., Birdwell, B., Boyle, M., Burgum, J. M., Burnham, J. A., Christian, E. R., Cook, W. R., Cooper, S. A., Cummings, A. C., Davis, A. J., Desai, M. I., Dickinson, J., Dirks, G., Do, D. H., Fox, N., Giacalone, J., Gold, R. E., Gurnee, R. S., Hayes, J. R., Hill, M. E., Kasper, J. C., Kecman, B., Klemic, J., Krimigis, S. M., Labrador, A. W., Layman, R. S., Leske, R. A., Livi, S., Matthaeus, W. H., McNutt, R. L., Mewaldt, R. A., Mitchell, D. G., Nelson, K. S., Parker, C., Rankin, J. S., Roelof, E. C., Schwadron, N. A., Seifert, H., Shuman, S., Stokes, M. R., Stone, E. C., Vandegriff, J. D., Velli, M., von Rosenvinge, T. T., Weidner, S. E., Wiedenbeck, M. E., and Wilson, P.: Integrated Science Investigation of the Sun (ISIS): Design of the Energetic Particle Investigation, Space Sci. Rev., 204, 187–256, doi:10.1007/s11214-014-0059-1, 2016.

Miteva, R.: On extreme space weather events: Solar eruptions, energetic protons and geomagnetic storms, Advances in Space Research, 66, 1977–1991, doi:https://doi.org/10.1016/j.asr.2020.07.006, URL https://www.sciencedirect.com/science/article/pii/S027311772030483X, 2020.

Miteva, R., Samwel, S. W., and Tkatchova, S.: Space Weather Effects on Satellites, Astronomy, 2, 165–179, doi:10.3390/astronomy2030012, URL https://www.mdpi.com/2674-0346/2/3/12, 2023.

Miteva, R., Samwel, S., and Dechev, M.: Energy Dependence of Solar Energetic Protons and Their Origin in Solar Cycles 23 and 24, Atmosphere, 15, doi:10.3390/atmos15081016, 2024.

Mitra, A. P.: Polar Cap Absorption Events, pp. 252–278, Springer Netherlands, Dordrecht, doi:10.1007/978-94-010-2231-6_11, URL https://doi.org/10.1007/978-94-010-2231-6_11, 1974.

Morosan, D. E., Zucca, P., Bloomfield, D. S., and Gallagher, P. T.: Conditions for electron-cyclotron maser emission in the solar corona, Astron. Astrophys., 589, L8, doi:10.1051/0004-6361/201628392, 2016.

Morosan, D. E., Kilpua, E. K. J., Carley, E. P., and Monstein, C.: Variable emission mechanism of a Type IV radio burst, Astron. Astrophys., 623, A63, doi:10.1051/0004-6361/201834510, 2019.

Moses, D., Droege, W., Meyer, P., and Evenson, P.: Characteristics of Energetic Solar Flare Electron Spectra, Astrophys. J., 346, 523, doi:10.1086/168034, 1989.

Müller, D., St. Cyr, O. C., Zouganelis, I., Gilbert, H. R., Marsden, R., Nieves-Chinchilla, T., Antonucci, E., Auchère, F., Berghmans, D., Horbury, T. S., Howard, R. A., Krucker, S., Maksimovic, M., Owen, C. J., Rochus, P., Rodriguez-Pacheco, J., Romoli, M., Solanki, S. K., Bruno, R., Carlsson, M., Fludra, A., Harra, L., Hassler, D. M., Livi, S., Louarn, P., Peter, H., Schühle, U., Teriaca, L., del Toro Iniesta, J. C., Wimmer-Schweingruber, R. F., Marsch, E., Velli, M., De Groof, A., Walsh, A., and Williams, D.: The Solar Orbiter mission. Science overview, Astron. Astrophys., 642, A1, doi:10.1051/0004-6361/202038467, 2020.

Müller-Mellin, R., Kunow, H., Fleissner, V., Pehlke, E., Rode, E., Röschmann, N., Scharmberg, C., Sierks, H., Rusznyak, P., Mckenna-Lawlor, S., Elendt, I., Sequeiros, J., Meziat, D., Sanchez, S., Medina, J., Peral, L., Witte, M., Marsden, R., and Henrion, J.: COSTEP - Comprehensive Suprathermal and Energetic Particle Analyser, Sol. Phys., 162, 483–504,

doi:10.1007/BF00733437, URL http://adsabs.harvard.edu/abs/1995SoPh..162..483M, 1995.

Müller-Mellin, R., Böttcher, S., Falenski, J., Rode, E., Duvet, L., Sanderson, T., Butler, B., Johlander, B., and Smit, H.: The Solar Electron and Proton Telescope for the STEREO Mission, Space Sci. Rev., 136, 363–389, doi:10.1007/s11214-007-9204-4, 2008.

Musset, S., Klein, K.-L., Fuller, N., Khreich, G., and Wargnier, A.: The time profile of relativistic solar particle events as observed by neutron monitors, Journal of Space Weather and Space Climate, 13, 15, doi:10.1051/swsc/2023016, 2023.

Núñez, M.: Predicting well-connected SEP events from observations of solar soft X-rays and near-relativistic electrons, Journal of Space Weather and Space Climate, 8, 1–10, doi:10.1051/swsc/2018023, 2018.

Ogilvie, K. W. and Desch, M. D.: The wind spacecraft and its early scientific results, Advances in Space Research, 20, 559–568, doi:10.1016/S0273-1177(97)00439-0, 1997.

Oka, M., Birn, J., Battaglia, M., Chaston, C. C., Hatch, S. M., Livadiotis, G., Imada, S., Miyoshi, Y., Kuhar, M., and Effenberger, F.: Electron Power-Law Spectra in Solar and Space Plasmas, Space Sci. Rev., 214, 82, doi:10.1007/s11214-018-0515-4, 2018.

Paassilta, M., Raukunen, O., Vainio, R., Valtonen, E., Papaioannou, A., Siipola, R., Riihonen, E., Dierckxsens, M., Crosby, N., Malandraki, O., Heber, B., and Klein, K.-L.: Catalogue of 55–80 MeV solar proton events extending through solar cycles 23 and 24, Journal of Space Weather and Space Climate, 7, A14, doi:10.1051/swsc/2017013, URL http://dx.doi.org/10.1051/swsc/2017013, 2017.

Paassilta, M., Papaioannou, A., Dresing, N., Vainio, R., Valtonen, E., and Heber, B.: Catalogue of {>} 55 MeV Wide-longitude Solar Proton Events Observed by SOHO, ACE, and the STEREOs at {≈} 1 AU During 2009 - 2016, Sol. Phys., 293, 70, doi:10.1007/s11207-018-1284-7, 2018.

Palmroos, C., Gieseler, J., Dresing, N., Morosan, D. E., Asvestari, E., Yli-Laurila, A., Price, D. J., Valkila, S., and Vainio, R.: Solar Energetic Particle Time Series Analysis with Python, Frontiers in Astronomy and Space Sciences, 9, 395, doi:10.3389/fspas.2022.1073578, 2022.

Palmroos, C., Dresing, N., Gieseler, J., Gutiérrez, C. P., and Vainio, R.: A new method for determining the onset times of solar energetic particles and their uncertainties: Poisson-CUSUM bootstrap hybrid method, Astron. Astrophys., 694, A221, doi:10.1051/0004-6361/202451280, 2025.

Papaioannou, A., Souvatzoglou, G., Paschalis, P., Gerontidou, M., and Mavromichalaki, H.: The First Ground-Level Enhancement of Solar Cycle 24 on 17 May 2012 and Its Real-Time Detection, Solar Physics, 289, 423–436, doi:10.1007/s11207-013-0336-2, URL https://doi.org/10.1007/s11207-013-0336-2, 2014.

Papaioannou, A., Sandberg, I., Anastasiadis, A., Kouloumvakos, A., Georgoulis, M. K., Tziotziou, K., Tsiropoula, G., Jiggens, P., and Hilgers, A.: Solar flares, coronal mass ejections and solar energetic particle event characteristics, Journal of Space Weather and Space Climate, 6, A42, doi:10.1051/swsc/2016035, 2016.

Papaioannou, A., Vainio, R., Raukunen, O., Jiggens, P., Aran, A., Dierckxsens, M., Mallios, S. A., Paassilta, M., and Anastasiadis, A.: The probabilistic solar particle event forecasting (PROSPER) model, J. Space Weather Space Clim., 12, 24, doi:10.1051/swsc/2022019, URL https://doi.org/10.1051/swsc/2022019, 2022.

Parker, E. N.: Dynamics of the Interplanetary Gas and Magnetic Fields., Astrophys. J., 128, 664, doi:10.1086/146579, 1958.

Posner, A.: Up to 1-hour forecasting of radiation hazards from solar energetic ion events with relativistic electrons, Space Weather, 5, 05001, doi:10.1029/2006SW000268, 2007.

Posner, A. and Strauss, R.: Warning Time Analysis From SEP Simulations of a Two-Tier REleASE System Applied to Mars Exploration, Space Weather, 18, e2019SW002354, doi:https://doi.org/10.1029/2019SW002354, URL https://agupubs.onlinelibrary.wiley.com/doi/abs/10.1029/2019SW002354, e2019SW002354 2019SW002354, 2020.

Priest, E. R. and Forbes, T. G.: The magnetic nature of solar flares, The Astronomy and Astrophysics Review, 10, 313–377, doi:10.1007/s001590100013, URL https://doi.org/10.1007/s001590100013, 2002.

Prikryl, P., Jayachandran, P. T., Mushini, S. C., and Richardson, I. G.: High-latitude GPS phase scintillation and cycle slips during high-speed solar wind streams and interplanetary coronal mass ejections: a superposed epoch analysis, Earth, Planets and Space, 66, 62, doi:10.1186/1880-5981-66-62, URL https://doi.org/10.1186/1880-5981-66-62, 2014.

Qin, G. and Wang, Y.: SIMULATIONS OF A GRADUAL SOLAR ENERGETIC PARTICLE EVENT OBSERVED BYHELIOS1,HELIOS2, ANDIMP8, The Astrophysical Journal, 809, 177, doi:10.1088/0004-637x/809/2/177, URL http://dx.doi.org/10.1088/0004-637X/809/2/177, 2015.

Raouafi, N. E., Patsourakos, S., Pariat, E., Young, P. R., Sterling, A. C., Savcheva, A., Shimojo, M., Moreno-Insertis, F., DeVore, C. R., Archontis, V., Török, T., Mason, H., Curdt, W., Meyer, K., Dalmasse, K., and Matsui, Y.: Solar Coronal Jets: Observations, Theory, and Modeling, Space Science Reviews, 201, 1–53, doi:10.1007/s11214-016-0260-5, URL http://dx.doi.org/10.1007/s11214-016-0260-5, 2016.

Ravishankar, A. and Michalek, G.: Relationship between solar energetic particle intensities and coronal mass ejection kinematics using STEREO/SECCHI field of view, Astron. Astrophys., 646, A142, doi:10.1051/0004-6361/202039537, 2021.

Reames, D. V.: Particle acceleration at the Sun and in the heliosphere, Space Sci. Rev., 90, 413–491, URL http://adsabs.harvard.edu/abs/1999SSRv...90..413R, 1999.

Reames, D. V.: Magnetic Topology of Impulsive and Gradual Solar Energetic Particle Events, The Astrophysical Journal, 571, L63, doi:10.1086/341149, URL https://dx.doi.org/10.1086/341149, 2002.

Reames, D. V.: The Two Sources of Solar Energetic Particles, Space Sci. Rev., 175, 53–92, doi:10.1007/s11214-013-9958-9, 2013.

Reames, D. V.: What Are the Sources of Solar Energetic Particles? Element Abundances and Source Plasma Temperatures, Space Science Reviews, 194, 303–327, doi:10.1007/s11214-015-0210-7, URL https://doi.org/10.1007/s11214-015-0210-7, 2015.

Reames, D. V.: Solar Energetic Particles. A Modern Primer on Understanding Sources, Acceleration and Propagation, vol. 978, Springer Cham, doi:10.1007/978-3-030-66402-2, 2021.

Reames, D. V. and Stone, R. G.: The identification of solar He-3-rich events and the study of particle acceleration at the sun, Astrophys. J., 308, 902–911, URL http://adsabs.harvard.edu/abs/1986ApJ...308..902R, 1986.

Reames, D. V., Barbier, L. M., and Ng, C. K.: The Spatial Distribution of Particles Accelerated by Coronal Mass Ejection–driven Shocks, Astrophys. J., 466, 473, doi:10.1086/177525, 1996.

Reber, G.: Cosmic Static., Astrophys. J., 100, 279, doi:10.1086/144668, 1944.

Richardson, I. G.: Solar wind stream interaction regions throughout the heliosphere, Living Reviews in Solar Physics, 15, 1, doi:10.1007/s41116-017-0011-z, 2018.

Richardson, I. G. and Cane, H. V.: Near-Earth Interplanetary Coronal Mass Ejections During Solar Cycle 23 (1996 - 2009): Catalog and Summary of Properties, Sol. Phys., 264, 189–237, doi:10.1007/s11207-010-9568-6, 2010.

Richardson, I. G., von Rosenvinge, T. T., Cane, H. V., Christian, E. R., Cohen, C. M. S., Labrador, A. W., Leske, R. A., Mewaldt, R. A., Wiedenbeck, M. E., and Stone, E. C.: $>$25 MeV Proton Events Observed by the High Energy Telescopes on the STEREO A and B Spacecraft and/or at Earth During the First $\sim$ Seven Years of the STEREO Mission, Sol. Phys., 289, 3059–3107, doi:10.1007/s11207-014-0524-8, 2014.

Rodgers, J. L. and Nicewander, W. A.: Thirteen Ways to Look at the Correlation Coefficient, The American Statistician, 42, 59–66, URL http://www.jstor.org/stable/2685263, 1988.

Rodríguez-García, L.: Acceleration and transport of solar energetic particles in the inner heliosphere, in: EGU General Assembly Conference Abstracts, EGU General Assembly Conference Abstracts, p. 6213, doi:10.5194/egusphere-egu24-6213, 2024.

Rodríguez-García, L., Gómez-Herrero, R., Zouganelis, I., Balmaceda, L., Nieves-Chinchilla, T., Dresing, N., Dumbović, M., Nitta, N. V., Carcaboso, F., dos Santos, L. F. G., Jian, L. K., Mays, L., Williams, D., and Rodríguez-Pacheco, J.: The unusual widespread solar energetic particle event on 2013 August 19. Solar origin and particle longitudinal distribution, Astron. Astrophys., 653, A137, doi:10.1051/0004-6361/202039960, 2021.

Rodríguez-García, L., Balmaceda, L. A., Gómez-Herrero, R., Kouloumvakos, A., Dresing, N., Lario, D., Zouganelis, I., Fedeli, A., Espinosa Lara, F., Cernuda, I., Ho, G. C., Wimmer-Schweingruber, R. F., and Rodríguez-Pacheco, J.: Solar activity relations in energetic electron events measured by the MESSENGER mission, Astron. Astrophys., 674, A145, doi:10.1051/0004-6361/202245604, 2023a.

Rodríguez-García, L., Gómez-Herrero, R., Dresing, N., Lario, D., Zouganelis, I., Balmaceda, L. A., Kouloumvakos, A., Fedeli, A., Espinosa Lara, F., Cernuda, I., Ho, G. C., Wimmer-Schweingruber, R. F., and Rodríguez-Pacheco, J.: Solar energetic electron events measured by MESSENGER and Solar Orbiter. Peak intensity and energy spectrum radial dependences: Statistical analysis, Astron. Astrophys., 670, A51, doi:10.1051/0004-6361/202244553, 2023b.

Rodríguez-García, L., Gómez-Herrero, R., Dresing, N., Balmaceda, L. A., Palmerio, E., Kouloumvakos, A., Jebaraj, I. C., Espinosa Lara, F., Roco, M., Palmroos, C., Warmuth, A., Nicolaou, G., Mason, G. M., Guo, J., Laitinen, T., Cernuda, I., Nieves-Chinchilla, T., Fedeli, A., Lee, C. O., Cohen, C. M. S., Owen, C. J., Ho, G. C., Malandraki, O., Vainio, R., and Rodríguez-Pacheco, J.: Solar energetic particles injected inside and outside a magnetic cloud: The widespread solar energetic particle event on 2022 January 20, Astron. Astrophys., 694, A64, doi:10.1051/0004-6361/202452158, 2025.

Rodríguez-Pacheco, J., Wimmer-Schweingruber, R. F., Mason, G. M., Ho, G. C., Sánchez-Prieto, S., Prieto, M., Martín, C., Seifert, H., Andrews, G. B., Kulkarni, S. R., Panitzsch, L., Boden, S., Böttcher, S. I., Cernuda, I., Elftmann, R., Espinosa Lara, F., Gómez-Herrero, R., Terasa, C., Almena, J., Begley, S., Böhm, E., Blanco, J. J., Boogaerts, W., Carrasco, A., Castillo, R., da Silva Fariña, A., de Manuel González, V., Drews, C., Dupont, A. R., Eldrum, S., Gordillo, C., Gutiérrez, O., Haggerty, D. K., Hayes, J. R., Heber, B., Hill, M. E., Jüngling, M., Kerem, S., Knierim, V., Köhler, J., Kolbe, S., Kulemzin, A., Lario, D., Lees, W. J., Liang, S., Martínez Hellín, A., Meziat, D., Montalvo, A., Nelson, K. S., Parra, P., Paspirgilis, R., Ravanbakhsh, A., Richards, M., Rodríguez-Polo, O., Russu, A., Sánchez, I., Schlemm, C. E., Schuster, B., Seimetz, L., Steinhagen, J., Tammen, J., Tyagi, K., Varela, T., Yedla, M., Yu, J., Agueda, N., Aran, A., Horbury, T. S., Klecker, B., Klein, K. L., Kontar, E., Krucker, S., Maksimovic, M., Malandraki, O., Owen, C. J., Pacheco, D., Sanahuja, B., Vainio, R., Connell, J. J., Dalla, S., Dröge, W., Gevin, O., Gopalswamy, N., Kartavykh, Y. Y., Kudela, K., Limousin, O., Makela, P., Mann, G., Önel, H., Posner, A., Ryan, J. M., Soucek, J., Hofmeister, S., Vilmer, N., Walsh, A. P., Wang, L., Wiedenbeck, M. E., Wirth, K., and Zong, Q.: The Energetic Particle Detector. Energetic particle instrument suite for the Solar Orbiter mission, Astron. Astrophys., 642, A7, doi:10.1051/0004-6361/201935287, 2020.

Samwel, S. and Miteva, R.: Correlations between space weather parameters during intense geomagnetic storms: Analytical study, Advances in Space Research, 72, 3440–3453, doi:https://doi.org/10.1016/j.asr.2023.07.053, URL https://www.sciencedirect.com/science/article/pii/S0273117723006026, 2023.

Santa Fe Dueñas, A., Ebert, R. W., Dayeh, M. A., Desai, M. I., Jian, L. K., Li, G., and Smith, C. W.: Dependence of Energetic Storm Particle Heavy Ion Peak Intensities and Spectra on Source CME Longitude and Speed, The Astrophysical Journal, 935, 32, doi:10.3847/1538-4357/ac73f5, URL https://doi.org/10.3847/1538-4357/ac73f5, 2022.

Schrijver, C. J.: Driving major solar flares and eruptions: A review, Advances in Space Research, 43,

739–755, doi:https://doi.org/10.1016/j.asr.2008.11.004, URL https://www.sciencedirect.com/science/article/pii/S0273117708005942, 2009.

Shibata, K., Masuda, S., Shimojo, M., Hara, H., Yokoyama, T., Tsuneta, S., Kosugi, T., and Ogawara, Y.: Hot-Plasma Ejections Associated with Compact-Loop Solar Flares, Astrophys. J. Lett., 451, L83, doi:10.1086/309688, 1995.

Sinclair, R. H. A. and Heather, R.: A review of solar type III radio bursts, Research in Astronomy and Astrophysics, 14, 773, doi:10.1088/1674-4527/14/7/003, URL https://dx.doi.org/10.1088/1674-4527/14/7/003, 2014.

Spearman, C.: The Proof and Measurement of Association between Two Things, The American Journal of Psychology, 15, 72–101, URL http://www.jstor.org/stable/1412159, 1904.

Spearman, C.: The proof and measurement of association between two things. By C. Spearman, 1904., The American journal of psychology, 100 3-4, 441–71, URL https://api.semanticscholar.org/CorpusID:40883791, 1987.

Stansby, D., Green, L. M., van Driel-Gesztelyi, L., and Horbury, T. S.: Active Region Contributions to the Solar Wind over Multiple Solar Cycles, Solar Physics, 296, doi:10.1007/s11207-021-01861-x, URL http://dx.doi.org/10.1007/s11207-021-01861-x, 2021.

Strauss, R. D., Dresing, N., Richardson, I. G., van den Berg, J. P., and Steyn, P. J.: On the Onset Delays of Solar Energetic Electrons and Protons: Evidence for a Common Accelerator, Astrophys. J., 951, 2, doi:10.3847/1538-4357/acd3ef, 2023.

Subramanian, K. R.: Radio Emission Processes: Part I, in: Heliophysical Processes, edited by Gopalswamy, N., Hasan, S., and Ambastha, A., pp. 137–151, Springer Berlin Heidelberg, Berlin, Heidelberg, 2010.

Thakur, N., Gopalswamy, N., Mäkelä, P., Akiyama, S., Yashiro, S., and Xie, H.: Two Exceptions in the Large SEP Events of Solar Cycles 23 and 24, Solar Physics, 291, 513–530, doi:10.1007/s11207-015-0830-9, URL https://doi.org/10.1007/s11207-015-0830-9, 2016.

Torsti, J., Valtonen, E., Lumme, M., Peltonen, P., Eronen, T., Louhola, M., Riihonen, E., Schultz, G., Teittinen, M., Ahola, K., Holmlund, C., Kelhä, V., Leppälä, K., Ruuska, P., and Strömmer, E.: Energetic Particle Experiment ERNE, Sol. Phys., 162, 505–531, doi:10.1007/BF00733438, 1995.

Tousey, R.: The solar corona., in: Space Research Conference, edited by Rycroft, M. J. and Runcorn, S. K., vol. 2, pp. 713–730, 1973.

Trotta, D., Pezzi, O., Burgess, D., Preisser, L., Blanco-Cano, X., Kajdic, P., Hietala, H., Horbury, T. S., Vainio, R., Dresing, N., Retinò, A., Marcucci, M. F., Sorriso-Valvo, L., Servidio, S., and Valentini, F.: Three-dimensional modelling of the shock–turbulence interaction, Monthly Notices of the Royal Astronomical Society, 525, 1856–1866, doi:10.1093/mnras/stad2384, URL https://doi.org/10.1093/mnras/stad2384, 2023.

Trotta, D., Larosa, A., Nicolaou, G., Horbury, T. S., Matteini, L., Hietala, H., Blanco-Cano, X., Franci, L., Chen, C. H. K., Zhao, L., Zank, G. P., Cohen, C. M. S., Bale, S. D., Laker, R., Fargette, N., Valentini, F., Khotyaintsev, Y., Kieokaew, R., Raouafi, N., Davies, E., Vainio, R., Dresing, N., Kilpua, E., Karlsson, T., Owen, C. J., and Wimmer-Schweingruber, R. F.: Properties of an Interplanetary Shock Observed at 0.07 and 0.7 au by Parker Solar Probe and Solar Orbiter, The Astrophysical Journal, 962, 147, doi:10.3847/1538-4357/ad187d, URL https://dx.doi.org/10.3847/1538-4357/ad187d, 2024.

Trottet, G., Samwel, S., Klein, K.-L., Dudok de Wit, T., and Miteva, R.: Statistical Evidence for Contributions of Flares and Coronal Mass Ejections to Major Solar Energetic Particle Events, Solar Physics, 290, 819–839, doi:10.1007/s11207-014-0628-1, URL http://dx.doi.org/10.1007/s11207-014-0628-1, 2014.

Trottet, G., Samwel, S., Klein, K. L., Dudok de Wit, T., and Miteva, R.: Statistical Evidence for Contributions of Flares and Coronal Mass Ejections to Major Solar Energetic Particle Events, Sol. Phys., 290, 819–839, doi:10.1007/s11207-014-0628-1, 2015.

Tylka, A. J.: New insights on solar energetic particles from Wind and ACE, Journal of Geophysical Research: Space Physics, 106, 25 333–25 352, doi:https://doi.org/10.1029/2000JA004028, URL

https://agupubs.onlinelibrary.wiley.com/doi/abs/10.1029/2000JA004028, 2001.

Tylka, A. J., Reames, D. V., and Ng, C. K.: Observations of systematic temporal evolution in elemental composition during gradual solar energetic particle events, Geophysical Research Letters, 26, 2141–2144, doi:https://doi.org/10.1029/1999GL900458, URL https://agupubs.onlinelibrary.wiley.com/doi/abs/10.1029/1999GL900458, 1999.

Vainio, R., Desorgher, L., Heynderickx, D., Storini, M., Flückiger, E., Horne, R. B., Kovaltsov, G. A., Kudela, K., Laurenza, M., McKenna-Lawlor, S., Rothkaehl, H., and Usoskin, I. G.: Dynamics of the Earth's Particle Radiation Environment, Space Science Reviews, 147, 187–231, doi:10.1007/s11214-009-9496-7, URL https://doi.org/10.1007/s11214-009-9496-7, 2009.

Vainio, R., Valtonen, E., Heber, B., Malandraki, O. E., Papaioannou, A., Klein, K.-L., Afanasiev, A., Agueda, N., Aurass, H., Battarbee, M., Braune, S., Dröge, W., Ganse, U., Hamadache, C., Heynderickx, D., Huttunen-Heikinmaa, K., Kiener, J., Kilian, P., Kopp, A., Kouloumvakos, A., Maisala, S., Mishev, A., Miteva, R., Nindos, A., Oittinen, T., Raukunen, O., Riihonen, E., Rodríguez-Gasén, R., Saloniemi, O., Sanahuja, B., Scherer, R., Spanier, F., Tatischeff, V., Tziotziou, K., Usoskin, I. G., and Vilmer, N.: The first SEPServer event catalogue ~68-MeV solar proton events observed at 1 AU in 1996-2010, Journal of Space Weather and Space Climate, 3, A12, doi:10.1051/swsc/2013030, 2013.

von Rosenvinge, T. T., Reames, D. V., Baker, R., Hawk, J., Nolan, J. T., Ryan, L., Shuman, S., Wortman, K. A., Mewaldt, R. A., Cummings, A. C., Cook, W. R., Labrador, A. W., Leske, R. A., and Wiedenbeck, M. E.: The High Energy Telescope for STEREO, Space Sci. Rev., 136, 391–435, doi:10.1007/s11214-007-9300-5, 2008.

Vourlidas, A., Lynch, B. J., Howard, R. A., and Li, Y.: How Many CMEs Have Flux Ropes? Deciphering the Signatures of Shocks, Flux Ropes, and Prominences in Coronagraph Observations of CMEs, Sol. Phys., 284, 179–201, doi:10.1007/s11207-012-0084-8, 2013.

Vršnak, B., Sudar, D., Ruždjak, D., and Žic, T.: Projection effects in coronal mass ejections, Astron. Astrophys., 469, 339–346, doi:10.1051/0004-6361:20077175, 2007.

Walton, S. D. and Murphy, K. R.: Superposed epoch analysis using time-normalization: A Python tool for statistical event analysis, Frontiers in Astronomy and Space Sciences, Volume 9 - 2022, doi:10.3389/fspas.2022.1000145, URL https://www.frontiersin.org/journals/astronomy-and-space-sciences/articles/10.3389/fspas.2022.1000145, 2022.

Wang, Y., Lyu, D., Wu, X., and Qin, G.: The Quantitative Relation of the Time Profiles of Intensities in the Well-connected Solar Energetic Particle Events, The Astrophysical Journal, 940, 67, doi:10.3847/1538-4357/ac99da, URL https://dx.doi.org/10.3847/1538-4357/ac99da, 2022.

Wang, Y.-M., Pick, M., and Mason, G. M.: Coronal Holes, Jets, and the Origin of 3He-rich Particle Events, The Astrophysical Journal, 639, 495, doi:10.1086/499355, URL https://dx.doi.org/10.1086/499355, 2006.

Warmuth, A.: Large-scale Globally Propagating Coronal Waves, Living Reviews in Solar Physics, 12, 3, doi:10.1007/lrsp-2015-3, 2015.

Webb, D. F. and Howard, T. A.: Coronal Mass Ejections: Observations, Living Reviews in Solar Physics, 9, 3, doi:10.12942/lrsp-2012-3, URL https://doi.org/10.12942/lrsp-2012-3, 2012.

Webb, D. F. and Jackson, B. V.: The identification and characteristics of solar mass ejections observed in the heliosphere by the HELIOS 2 photometers, J. Geophys. Res., 95, 20 641–20 661, doi:10.1029/JA095iA12p20641, 1990.

White, S. M.: Solar Radio Bursts and Space Weather, arXiv e-prints, arXiv:2405.00959, doi:10.48550/arXiv.2405.00959, 2024.

Wibberenz, G. and Cane, H. V.: Multi-Spacecraft Observations of Solar Flare Particles in the Inner

Heliosphere, Astrophys. J., 650, 1199–1207, URL http://adsabs.harvard.edu/abs/2006ApJ...650.1199Wzotero://attachment/116/, 2006.

Wilson, Lynn B., I., Brosius, A. L., Gopalswamy, N., Nieves-Chinchilla, T., Szabo, A., Hurley, K., Phan, T., Kasper, J. C., Lugaz, N., Richardson, I. G., Chen, C. H. K., Verscharen, D., Wicks, R. T., and TenBarge, J. M.: A Quarter Century of Wind Spacecraft Discoveries, Reviews of Geophysics, 59, e2020RG000 714, doi:10.1029/2020RG000714, 2021.

Wraase, S., Heber, B., Böttcher, S., Bucik, R., Dresing, N., Gómez-Herrero, R., Klassen, A., and Müller-Mellin, R.: Interpretation of increased energetic particle flux measurements by SEPT aboard the STEREO spacecraft and contamination, Astron. Astrophys., 611, A100, doi:10.1051/0004-6361/201732063, 2018.

Zheleznyakov, V. V. and Zaitsev, V. V.: The Origin of Type-V Solar Radio Bursts., Soviet Astronomy, 12, 14, 1968.

Zimbardo, G., Ying, B., Nisticò, G., Feng, L., Rodríguez-García, L., Panasenco, O., Andretta, V., Banerjee, D., Bemporad, A., De Leo, Y., Franci, L., Frassati, F., Habbal, S., Long, D., Magdalenic, J., Mancuso, S., Naletto, G., Perri, S., Romoli, M., Spadaro, D., Stangalini, M., Strachan, L., Susino, R., Vainio, R., Velli, M., Cohen, C. M. S., Giacalone, J., Shen, M., Telloni, D., Abbo, L., Burtovoi, A., Jerse, G., Landini, F., Nicolini, G., Pancrazzi, M., Russano, G., Sasso, C., and Uslenghi, M.: A high-latitude coronal mass ejection observed by a constellation of coronagraphs: Solar Orbiter/Metis, STEREO-A/COR2, and SOHO/LASCO, Astron. Astrophys., 676, A48, doi:10.1051/0004-6361/202346011, 2023.

Zurbuchen, T. H. and Richardson, I. G.: In-Situ Solar Wind and Magnetic Field Signatures of Interplanetary Coronal Mass Ejections, Space Sci. Rev., 123, 31–43, doi:10.1007/s11214-006-9010-4, 2006.

TURUN
YLIOPISTO
UNIVERSITY
OF TURKU

Painosalama, Turku, Finland 2026

ISBN 978-952-02-0627-7 (PRINT)
ISBN 978-952-02-0628-4 (PDF)
ISSN 0082-7002 (Print)
ISSN 2343-3175 (Online)